Protocol of Measurement Techniques

August 2004

Project
Colored Solar Collectors
Capteurs solaires en couleur

author and coauthors	Dr. Andreas Schüler, Estelle De Chambrier, Christian Roecker, Prof. Dr. Jean-Louis Scartezzini
institution	Ecole Polytechnique de Lausanne EPFL Laboratoire d'Energie Solaire et de Physique du Bâtiment LESO-PB
address	Bâtiment LE, 1015 Lausanne
phone, email, webpage	(021) 693 4544, andreas.schueler@epfl.ch, estelle.dechambrier@epfl.ch http://lesowww.epfl.ch

ABSTRACT

The architectural integration of thermal solar collectors into buildings is often limited by their black color, and the visibility of tubes and corrugations of the absorber sheets. A certain freedom in color choice would be desirable, but the colored appearance should not cause excessive energy losses. Multilayered thin film interference filters on the collector glazing can produce a colored reflection, hiding the corrugated metal sheet, while transmitting the non-reflected radiation entirely to the absorber. The proposed colored glazed solar collectors will be ideally suited for architectural integration into buildings, e.g. as solar active glass facades.

For the considered application, suitable coatings shall be developed by a sol-gel dip-coating process. These coatings should thus produce a visible reflection in a certain variety of possible color shades while keeping the solar transmission as high as possible. Additionally, the colored coatings will have to meet high durability requirements.

Within this project, multilayered thin film interference stacks will have to be designed and realized. The proper combinations of refractive indices and film thicknesses will have to be chosen. The corresponding multilayered thin film stacks will have to be realized experimentally in a controlled and reproducible way. New thin film materials shall be tailored to exhibit optimized optical and aging properties. The aging properties of the deposited films will have to be optimized. The development of these coatings will be based on various measurement techniques, such as spectrophotometry, measurements of total power throughput by means of a solar simulator, spectroscopic ellipsometry, scanning electron microscopy (SEM), X-ray diffraction (XRD) and X-ray photoelectron spectroscopy (XPS). Giving many examples for typical data this protocol explains which film properties can be inferred from each method and describes thus both function and purpose of the different measurement techniques.

BFE
OFEN
UFE
SFOE

Contents

1 Introduction

Architectural integration of solar energy systems into buildings is becoming more and more important. Thermal solar collectors, typically equipped with black, optical selective absorbers sheets, exhibit in general good energy conversion efficiencies. However, the black color, and sometimes the visibility of tubes and corrugations of the metal sheets, limits the architectural integration into buildings.

Our approach to this problem is to fabricate a glazing which reflects a narrow spectral band in the visible range of the sunlight and is transparent for the rest of the solar spectrum, thereby minimizing the energy losses. All the energy which is not reflected, should be transmitted, therefore no absorption should occur at all. While coloring the bulk glass leads to beautiful colors of the transmitted light (in general by absorption), it leads only to a weak modification of the color of the reflected light. However, there is only little light to transmit in front of a black solar absorber. In order to color the reflected light, thin film interference is to be considered, well known from soap bubbles, thin oil films on water, etc.. The cover glass of the collector should be coated, either on one side, or on both. Because of the constraint that no absorption must occur, these thin films have to been build up of dielectric, transparent materials like e.g. SiO_2, Al_2O_3, TiO_2, or mixtures of those. Of course the glass to be coated should be practically iron-free ('white' solar glass).

Within this project, suitable multilayered coatings shall be developed by a sol-gel dip-coating process. These coatings should thus produce a visible reflection in a certain variety of possible color shades while keeping the solar transmission as high as possible. Additionally, the colored coatings will have to meet high durability standards.

For a controlled sol-gel deposition of multilayers, the optical properties of the thin film materials have to be known precisely. **Spectrophotometry** can be used for the determination of the refractive index n and the extinction coefficient k. **Spectroscopic Ellipsometry** allows to infer those numbers with an even higher precision. Both methods are also used to establish the relation of film thickness and withdrawal speed for each precursor solution, which is essential for the controlled multilayer deposition by sol-gel dip-coating.

The energy-efficiency of the colored reflection produced by the multilayered samples is characterized by the visible reflectance as determined by spectrophotometry, and by the solar transmission as measured directly by a **solar simulator in combination with a thermopile detector**. The ratio of the visible reflectance and the solar energy losses serves hereby as a figure of merit.

The quantification of the achieved colors, the color saturation, the angle-dependence and aging stability of the colors is provided by **colorimetry**, which is either based on measured reflectance or transmittance spectra or on three sensor colorimetric devices. Another application of spectrophotometry is the measurement of light scattering by the sample.

The coatings to be developed will have to meet high durability requirements. X-ray-diffraction will allow to identify the present crystalline phases, to measure the crystallite sizes and to assess the texture of the films, information which is highly relevant for the optimization of aging properties. As important as that is the morphology of the film growth, as observed by **Scanning electron microscopy (SEM)**. While the production of porous films favors a low index of refraction and thus a high solar transmission, the production of dense films enhances the coating durability. Detecting surface and interface roughness and in some cases also pores and voids, scanning electron microscopy will also be very helpful for the interpretation of the optical measurements. Additionally, for the controlled deposition of multilayers it will be very useful to check whether film morphology changes while adding layers, and to check layer thicknesses by cross sectional micrographs.

The correlation between the chemical composition of the deposited thin films and the chemical composition of the precursor solution is essential in order to establish the desired optical properties. **X-ray photoelectron spectroscopy (XPS)** will allow to determine the thin film composition, which can be compared to the volume ratios used for the solution synthesis.

The various experimental methods are described in the different chapters of this protocol. Due to the importance of the technique and its accessibility in our laboratory, the aspects related to spectrophotometry have been discussed especially in detail.

2 Spectrophotometry

In the following chapter, the equipment and techniques used for spectrophotometry are described. Various configurations of the spectrometer allow measurements of diffuse and specular transmission, reflection and absorption. These measurements allow to generate experimental data for the determination of the optical properties refractive index n, the index of extinction k and the film thickness d (see Chapter 3) as well as for the quantification of colors (see Chapter 4).

2.1 Description of Instrument

2.1.1 Technical Data

Spectrograph: MultiSpec 125^{TM} 1/8m, Oriel, model 77400

PDA camera: Instaspec II ^{TM} detector head, model 77090

Software: InstaSpec^{TM} II

Figure 2.1: The spectrophotometer consisting of the sighting optics, the unit containing the dispersion optics and the detector. The photograph shows also the computer for the data acquisition (software " Instaspec II ").

The spectrophotometer is composed of three main components: the sighting optics, the unit containing a diffraction grating as the heart of the dispersion optics, and the detector head.

2.1.2 Sighting Optics

The sighting optics focuses the incoming light on the entrance slit, which is typically a few tens of micrometers wide and 2 or 3 mm high. A beam splitter in combination with a sighting ocular allows the spectrometer to be aligned with objects by eye. The incoming light is limited by the acceptance angle described as the numerical aperture (or F number) of the spectrograph.

2.1.3 Unit of Dispersion Optics

A diffraction grating is used to break up the light into components of different wavelengths. The plane gratings are interchangeable allowing great versatility in the selection of the measurable wavelength range. The grating position can be adjusted by a micrometer drive providing a mechanical calibration of the instrument.

Instead of using an exit slide, the optics has a wide aperture which gives a light distribution dispersed over the full area of the photodiode array detector.

2.1.4 Detector Head

The detector head consists of an array of sensors. In general, two main arrays are used: silicon photodiode arrays (PDAs) and charge coupled devices (CCDs).

The detector coupled to our spectrograph consists of a PDA with 1024 photodiode array elements. In the PDA, the individual photodiodes are arranged in a linear array and linked to electronic FET switches allowing one diode to be read at a time. The analog signal read through each FET correlates to the amount of light incident on the pixel. The usable wavelength range of the silicon based multichannel detector (Intaspec II model 77090), extends from approximately 180 nm to 1100 nm. In order to reduce the thermal background, the detector head contains a cooling system for temperature stabilization. Thermoelectric coolers and cooling fins are used to maintain the temperature of the array at a constant value, which can be programmed in the range of –10°C to +30°C.

2.1.6 Software

The InstaSpec™ II software controls the photodiode array hardware as well as the display of graphics, data manipulation and file storage.

Measurement parameters (e.g. integration time, choice of grating, working temperature) can be created and stored as specific configurations. Measurement modes acquire data in units of Counts, percent of Transmittance, or percent of Reflectance. The thermal background can be subtracted from the signal. The software provides also the option of instantaneous baseline division (division by a reference spectrum).

2.2 Calibration

Before spectroscopic measurements, and especially after a change in the experimental configuration (e.g. a change of the grating), a wavelength calibration of the spectrophotometer may be needed. For this procedure, spectral calibration lamps are used which produce narrow spectral lines ("Pencil Style" mercury and rare gas sources, ORIEL).

Fig. 2.2 shows a Hg(Ar) lamp spectrum presenting a limited set of narrow and well defined lines. Knowing the theoretical wavelength position of those lines, the spectrophotometer can easily be calibrated either mechanically by adjusting the micrometer screw or digitally by adapting the corresponding values in the software.

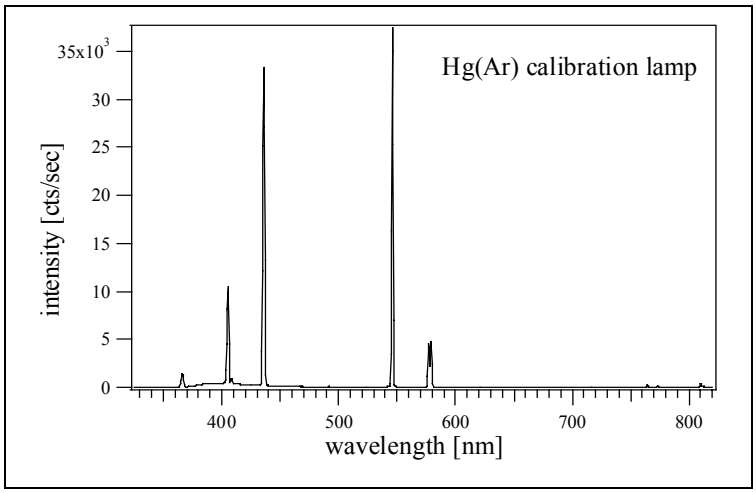

Figure 2.2: Hg(Ar) lamp spectral lines. The main peaks at λ = 435 and 546 nm and their second order signals are a convenient choice for the wavelength calibration.

2.3 Gratings

Ruled gratings are typically made of a substrate with large number of parallel grooves ruled in its surface and overcoated with reflected materials such as aluminium. Spacing and quality of the grooves determine the specifications and the performances of the grating. Holography can also be used for the fabrication of diffraction gratings.

2.3.1 Grating Equation

Based on the principle of constructive interference, a basic grating equating can be derived:

$$a(\sin\alpha+\sin\beta)=m\lambda \qquad \textbf{Equation 2.1}$$

with λ the wavelength of light , a the distance between two adjacent grooves (called the groove spacing), α the angle of incidence, β the angle of diffraction, m an integer (the order of diffraction).

For a monochromatic light beam incident on the grating constructive interference occurs in defined directions governed by equation 2.1. As either the wavelength or the order of diffraction are increased, the angle of diffraction, β, increases. Therefore, polychromatic light diffracted by such a grating will be dispersed.

2.3.2 Resolution and Resolving Power

Resolution in spectral measurements refers to the measure of the ability of the instrument to separate two spectral lines which are close together.

The Resolving Power R of a grating is defined in terms of wavelengths λ and $\lambda + \delta\lambda$, where $\lambda + \delta\lambda$ is the closest wavelength to λ which can be resolved. Theoretically, from the grating equation:

$$R=\frac{\lambda}{\delta\lambda}=\frac{W(\sin\alpha+\sin\beta)}{\lambda}=\frac{mW}{a} \qquad \textbf{Equation 2.3}$$

where $\delta\lambda$ is the resolution and W the illuminated width of the grating.

Thus the resolution of the grating is inversely proportional to the groove spacing. Hence a smaller groove spacing (a grating with more lines/mm) gives higher resolution. However with more lines/mm the bandwidth of the whole spectra is reduced.

2.3.3 Grating Characteristics

Three different gratings are used to do spectrometric measurements: a 600 lines/mm grating (Oriel model 77414) which has a primary wavelength region of 180 to 500 nm and a resolution of around 0.8 nm (for 25 μm wide entrance slit), a 400 lines/mm grating (model 77416) with a region of 250 to 1300 nm giving a resolution of 1 nm and a 150 lines/mm grating (model 77967) ranging theoretically from 190 to 800 nm with a resolution of around 5 nm. For this last one, some experiments showed that spectral signals can be trusted up to a wavelength of 1000 nm.

2.4 Saturation of the Detector

For many sensors a linear range exists; as the input is increased however, the output saturates to a constant value. Similar behaviour is shown by the spectrometer.

Saturation charge is the largest signal that can be measured and is due to the limited well depth capacity of the pixel. It is quoted in electrons or coulombs. Due to the large unit area of their pixels, PDAs detectors have a large saturation level.

The saturation level of our InstaspecII Silicon PDA detector is 125 x 10^6 e^- and corresponds to a signal of around 58 000 counts. For every measurement, care has to be taken in order to work in the linear regime thus ensuring that the output is not saturated for any wavelength.

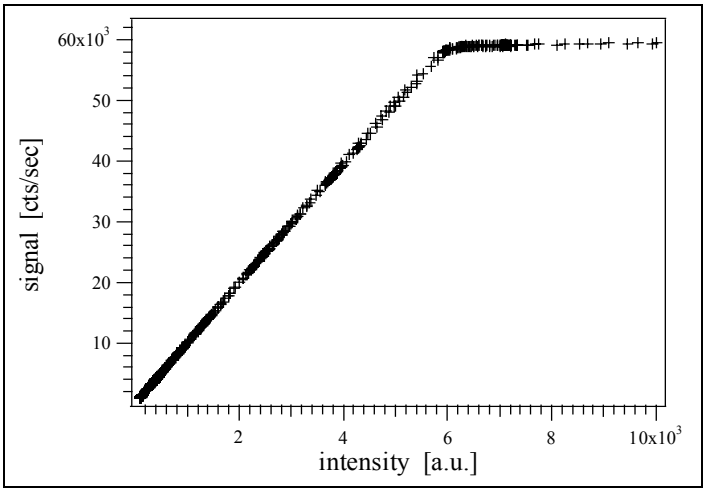

Figure 2.3: Measured output signal vs. input intensity. The plot clearly shows the linear regime and the saturation of the spectrometer output. Saturation occurs at around 58 ·10^3 [cts/sec].

2.5 Alignment

When doing spectral measurements, care has to be taken with the alignment of the optical part at the entrance of the spectrograph, i.e. the position of the entrance slit. Tilting the slit or moving it out of the focus of the first mirror has significant effects on the results, particularly on their resolution. Examples of misalignments are given in Fig. 2.4 for a line of the Hg(Ar) calibration lamp.

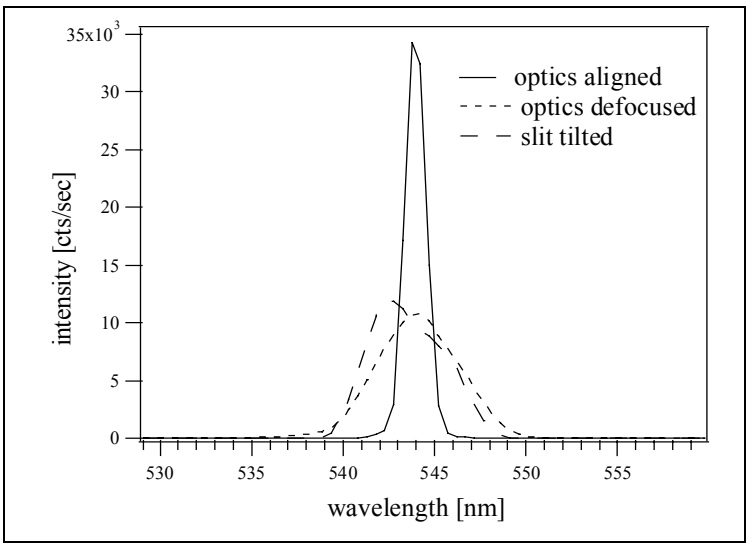

Figure 2.4: Zoom on a spectral line of a Mercury-Argon lamp. The sighting optics was moved so that the entrance slit was tilted and moved out of the focus. The corresponding spectra exhibit a line broadening due to the misalignment.

2.6 Diffraction Maxima Of Higher Order

2.6.1 Diffraction Orders

We have previously introduced the grating equation as:

$$a(\sin\alpha+\sin\beta)=m\lambda \qquad \textbf{Equation 2.1}$$

with the groove spacing a, the angle of incidence α, the angle of diffraction β, and the order of diffraction m.

For a particular groove spacing, angle of incidence and angle of reflection, the grating equation is satisfied by more than one wavelength. With these parameters (a, α and β) held constant and m increasing in successive integers, constructive interference will occur for a series of discrete wavelengths.

For constructive reinforcement of waves diffracted by successive grooves, it is required that the rays are delayed or advanced in phase with respect to one another by 2π. This phase difference corresponds to a real distance, the path difference, which equals an integral multiple of the wavelength. The first diffraction order (m = 1, -1) corresponds to the path difference between waves diffracted from successive grooves being equal to one wavelength. Similarly, the second order (m = 2, -2) corresponds to a path difference of two wavelengths between the rays diffracted from adjacent grooves. The case m = 0 corresponds to specular reflection ($\alpha = -\beta$).

2.6.2 Overlapping of Diffracted Spectra

The most troublesome aspect of multiple order diffraction is that successive spectra overlap. It is evident from the grating equation that the light of wavelength λ diffracted in the m = 1 order will coincide with the light of wavelength $\lambda/2$ diffracted in the m = 2 order, and so on.

This superposition of spectra is present in every measurement and would lead to incorrect data if not taken into account and prevented.

Looking at the dispersion equation (equation 2.2) it is obvious that the dispersion of the second order is twice the dispersion of the first order, the third order three times, etc. The first order is usually the strongest, and so the most interesting one. The higher orders have to be blocked in order to avoid false signals.

Filters are used for this purpose of order sorting.

Whether an order sorting filter is needed, and if so which one, depends on both the spectral output of the source and the spectral range under study.

2.6.3 Red Filter for Order Sorting

In order to avoid high order maxima signals, two spectra are taken, with and without an order sorting filter. Both spectra are thereafter combined to give data free of higher ordered diffraction peaks.

For illustration of the technique, see Figs. 2.5 and 2.6. A transmission measurement of a given thin film sample (titanium dioxide on glass) has been taken without any filter. A grating with

150 lines/mm has been used. Then a red filter, which stops radiation with wavelengths below 550 nm, is placed between the source and the sample is measured again. The non-filtered and filtered spectra are then combined into one, thus omitting the artefacts due to the cut-off of the red filter (thermal noise below 550 nm) and due to the second order diffraction (above 700 nm).

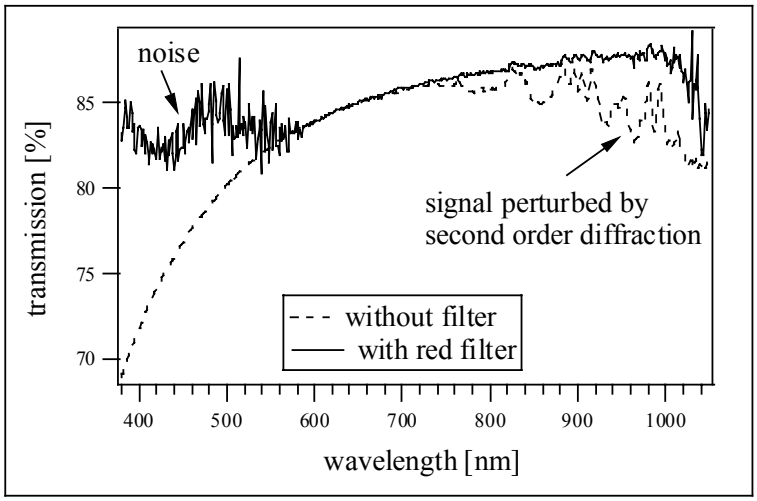

Figure 2.5: Transmission spectra of a TiO_2 film on glass measured with and without a red filter. The spectrum measured without filter shows a second order diffraction signal above 700 nm. The red filter cuts the radiation with wavelengths below 550 nm. Consequently, also the second order signals are suppressed up to a wavelength of 1100 nm.

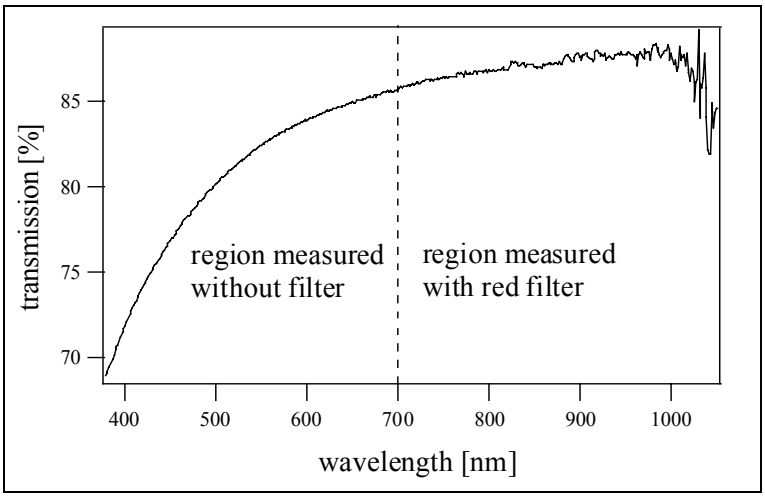

Figure 2.6: The combination of the two spectra with and without red filter. This kind of combined plot yields broad ranging spectra free from the artefacts due to higher order diffraction.

2.7 Measurements Configurations

This section reviews different experimental configurations for the optical characterization of thin film samples, such as reflectance and transmittance (diffuse and specular under various angles of incidence). In addition to colorimetric purposes (Chapter 4), these measurements allow to generate experimental data for the determination of the optical properties refractive index n, the index of extinction k and the film thickness d (Chapter 3).

2.7.1 Direct Transmittance Measurements

The sample is placed between the source of illumination and the spectrophotometer. By a careful, laser-supported alignment procedure, the thin film is positioned perpendicularly to the beam (angle of incidence equal to zero). An example of such a measurement is given in Fig. 2.8, designed by an angle $\theta = 0$. The reference spectrum used to evaluate the transmission is simply the spectrum measured after removal of the sample.

2.7.2 Variable Angle Transmittance Measurements

For this kind of measurements, the incidence angle is varied from 0° to 70°. A rotational sample holder has been specifically designed for this purpose, allowing angles to be set precisely. This sample holder adapts to different substrates thicknesses thus assuring that the sample is always centered on the axis of rotation.

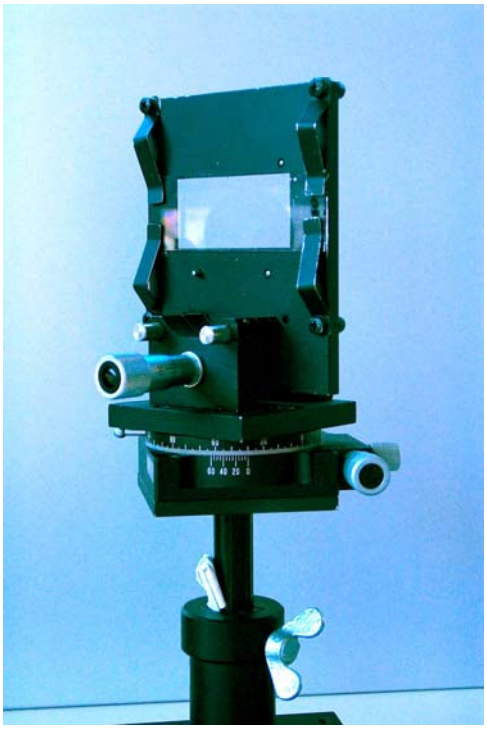

Figure 2.7: Sample holder for transmittance versus angle measurements. The angle of incidence can be set very accurately.

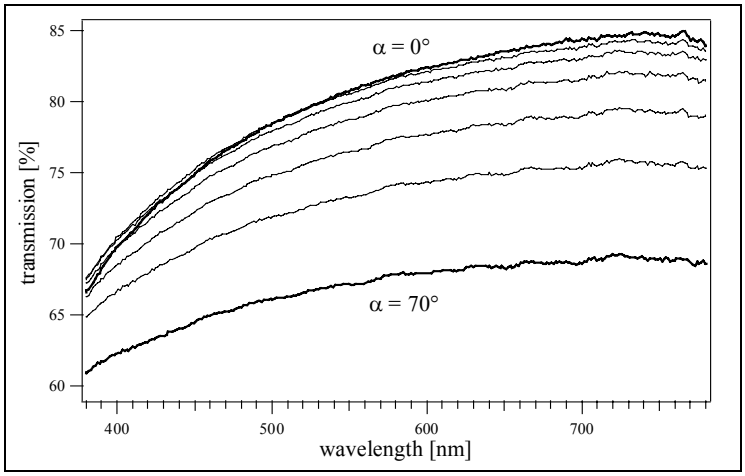

Figure 2.8: Transmittance versus angle measurement of a TiO_2 film on glass.

2.7.3 Variable Angle Reflectance Measurements

For the measurement of the specular reflectance with varying angle of incidence a special experimental setup has been designed and constructed (see Fig. 2.9). A special mechanics divides the angle between the two arms of the apparatus, thus guaranteeing the alignment with respect to the angles of incidence and reflection. Samples are compared to a well-defined silicon reference sample. The data directly measured from the sample are corrected by a multiplication with the theoretical reflectance values for silicon (Fig. 2.10). The latter have been computed for the optical constants given in ref. [PAL98]

As an example, the experimental result for of a TiO_2 thin film is illustrated in Fig. 2.11 (reflection angles between 2.5° and 70°).

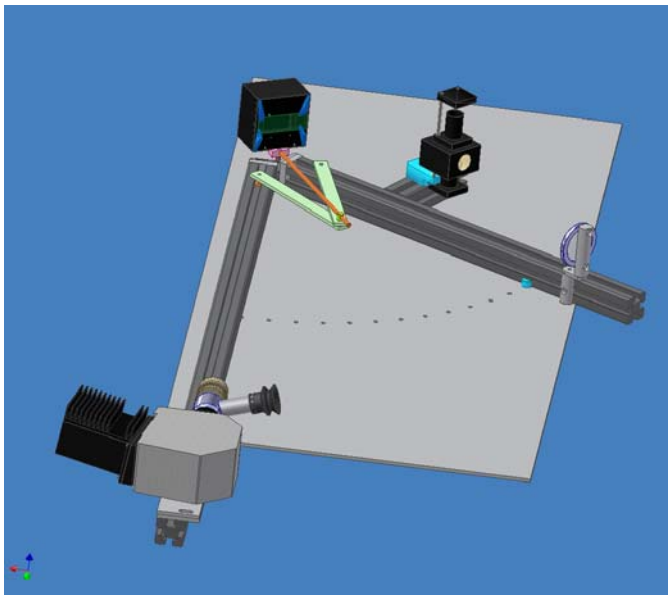

Figure 2.9: Apparatus for the variable angle reflectance measurements: The source illuminates a white lambertian surface. The reflection of the latter is captured by the sighting optics of the spectrophotometer. In a first step, a reference is taken with the silicon wafer positioned in the sample holder, then the sample is put into place and a measurement recorded. Drawing by P. Loesch, LESO, EPFL.

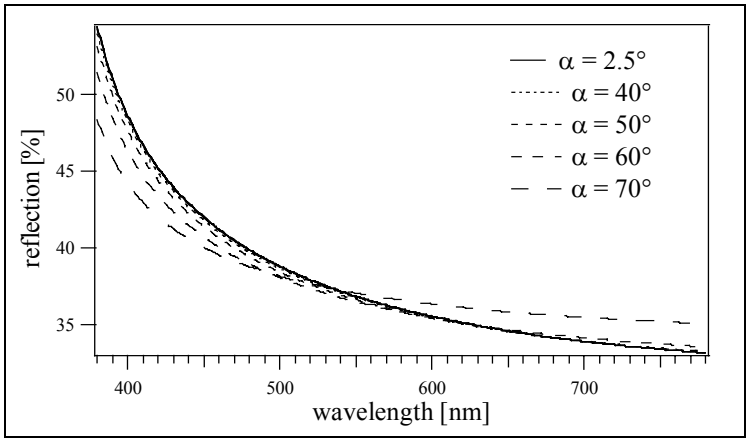

Figure 2.10: Theoretical data for the angle-dependent reflectance of silicon used as reference values for the experiments. The reflectance data have been calculated using the optical constants given in ref. [PAL98].

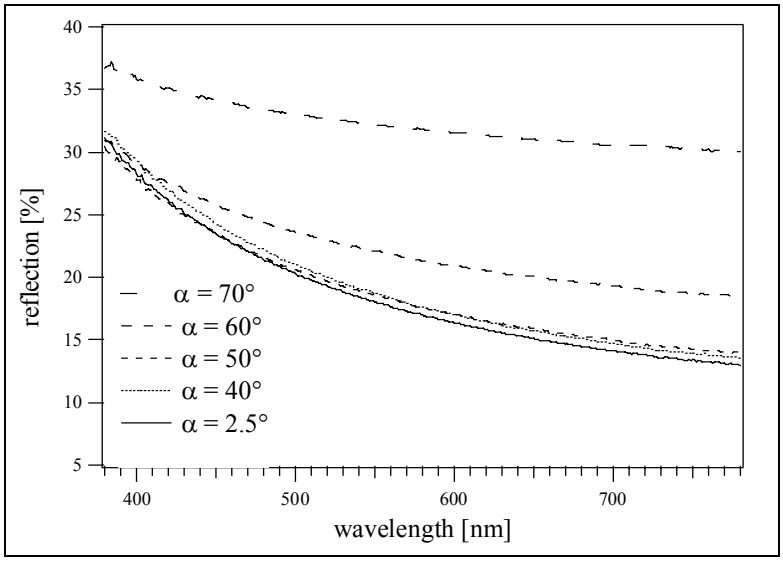

Figure 2.11: Experimental data for the angle-dependent reflectance of a TiO_2 sample after correction with the theoretical values for the silicon reference.

2.7.4 Integrating Sphere

An integrating sphere is used for the measurements of diffuse and total hemispherical transmittance and reflectance. Reflected or transmitted light is collected, uniformly reflected and scattered around the sphere's white interior. The output measured by means of the spectrophotometer represents the angle-integration of the light transmitted or reflected by the sample within the complete hemisphere.

The interior of the integrating sphere used in our experiments is coated with a very stable barium sulphate based white coating. This coating is highly reflective, > 95%, in the visible.

As it is important to have a parallel, well collimated beam at the entrance of the sphere, an optical bench is assembled between the source and the sphere. A picture of the optical bench and the integrating sphere is shown is Fig. 2.12.

2.7.5 Diffuse and Total Transmittance Measurements

Direct transmittance does not measure light eventually scattered by the sample. This drawback can be overcome by a measurement of the diffused light using an integrating sphere. In this experimental configuration, the thin film is put at the entrance of the sphere, and measures the total hemispherical transmittance (total = diffuse + specular). An example is shown in Fig. 2.13. By creating an exit opening for the specular transmitted light, it is even possible to measure the diffuse transmission only.

2.7.6 Diffuse Reflectance Measurements

The total hemispherical reflectance (diffuse reflectance + specular reflectance) is the counterpart of the total transmittance. In absence of absorption both are complementary in the sense that their sum equals 100%. If both total reflectance and transmittance are known, the percentage of absorption within the sample can be easily inferred.

For a measurement of the diffuse or the total hemispherical reflectance, an opening with a sample holder is provided opposing the sphere's entrance.

Care has to be taken to avoid any unwanted reflection coming from the outside and transmitting the sample. The reference measurements are taken with a white surface in place of the sample.

In order to measure only the diffuse reflectance (total reflectance minus specular reflectance), a black optical cavity (light trap) is placed in the way of the direct reflected beam, thus eliminating the direct component. Measurements of both the total and the diffuse only hemispherical reflectance are shown in Fig. 2.13.

REFERENCES

[PAL98] E.D. Palik, *Handbook of optical constants of solids*, vol. 1-3, Academic Press (1998)

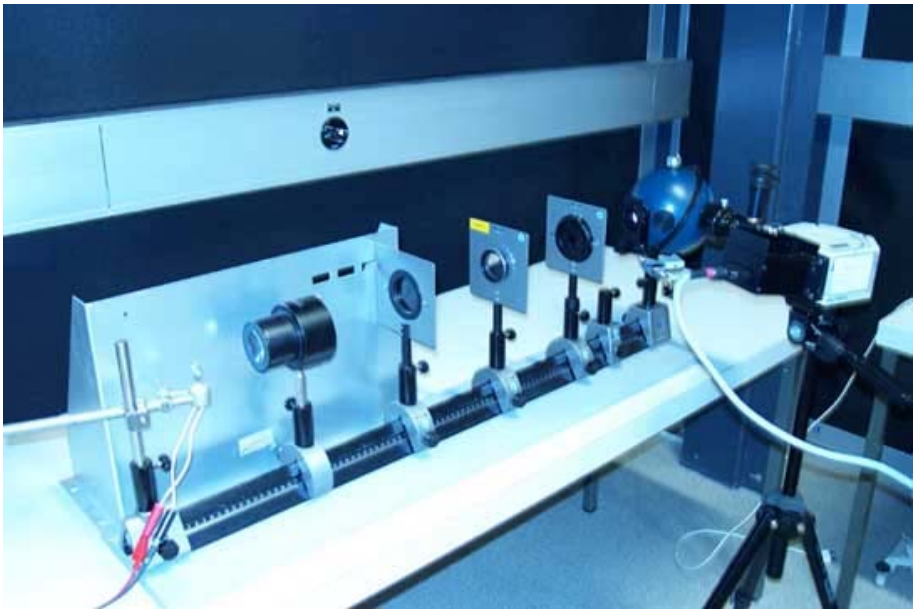

Figure 2.12: Integrating sphere, spectrophotometer and optical bench. The light emitted by a halogen lamp is collimated before reaching the integrating sphere.

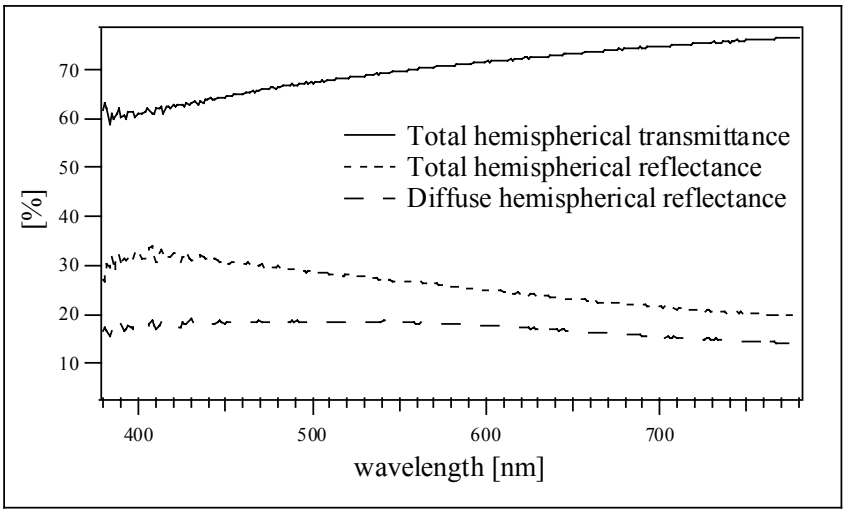

Figure 2.13: Examples of measurements using the integrating sphere. Shown are the diffusive reflectance, the total hemispherical reflectance and the total hemispherical transmittance of a TiO_2 film deposited on glass.

3 Determination of Refractive Index and Film Thickness

For the fabrication of multilayer interference stacks, a precise knowledge on the optical constants of the used materials as well as the possibility to control the film thicknesses of the individual layers are essential. In order to control a sol-gel dip-coating process, it is extremely important to establish the relation between the film thickness and the withdrawal speed for the precursor solution of a given viscosity, density and surface tension.

Therefore, in order to design an optimal multilayered interference coating, an optical characterisation of the individual layers is essential. In this chapter different methods are described for the determination of the refractive index, extinction coefficient and layer thickness of a thin film.

3.1 Preliminary Considerations

3.1.1 Introduction of n, k and d

The complex refractive index is given by N = n – ik, with the refractive index n familiar from Snell's law and the extinction coefficient k. A nonzero value of k denotes the presence of absorption within the medium. In order to avoid energy losses within the coatings on the solar collector glazing, the absorption within the thin films should be negligible. An extinction coefficient of k= 0 is thus desired.

The complex dielectric function $\varepsilon(\lambda)$ equals the square of the complex refractive index $N(\lambda)$.

The thickness of the considered thin film will be denoted by d.

3.1.2 Substrate with Two Identically Coated Sides vs. Individual Coated Surface

Within a transparent substrate, infinite multiple reflections occur between the two sides. In the absence of absorption and scattering, it can be shown for a substrate, which is coated identically on both sides, that

$$r=\frac{R}{(2-R)} \qquad \textbf{Equation 3.1}$$

where R is the specular reflectance of the total system, and r is the specular reflectance due to one coated surface only.

A similar expression holds for the specular transmittance T of the total system and the transmission t of one coated surface :

$$t=\frac{2T}{(1+T)} \qquad \textbf{Equation 3.2}$$

3.1.3 Determination of the Refractive Index of the Glass Substrate

The transmission t at the interface between a non-absorbing medium, with refractive index n_0 , and an infinite transparent glass of refractive index n_1 , is given by the following expression [KNI76] :

$$t=\frac{4n_1n_0}{(n_1+n_0)^2} \qquad \textbf{Equation 3.3}$$

In the case of air as the incident medium n_0 is equal to 1.

By inverting equation 3.3, the following relation is found:

$$n=-(1-\frac{2}{t})\pm\sqrt{\left(1-\frac{2}{t}\right)^2-1} \qquad \textbf{Equation 3.4}$$

The transmission t at one interface can be inferred from the transmission of the total system by equation 3.2.

By taking a transmittance (or reflectance) spectrum of an uncoated substrate, the dispersion relation $n(\lambda)$ can be evaluated with equation 3.4. Hereby, the positive or negative square root has to be chosen, according to the physical constraints for n. Fig. 3.1 shows the measured data for the transmission T of the glass substrate, while Fig. 3.2 displays the inferred values for the refractive index n. A smoothed curve is added to the figure.

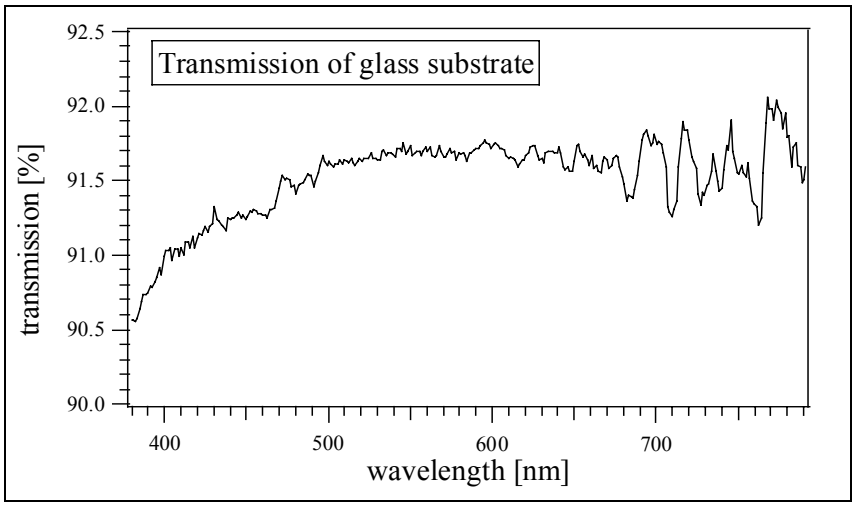

Figure 3.1: Measured transmission of a glass substrate (microscope slide).

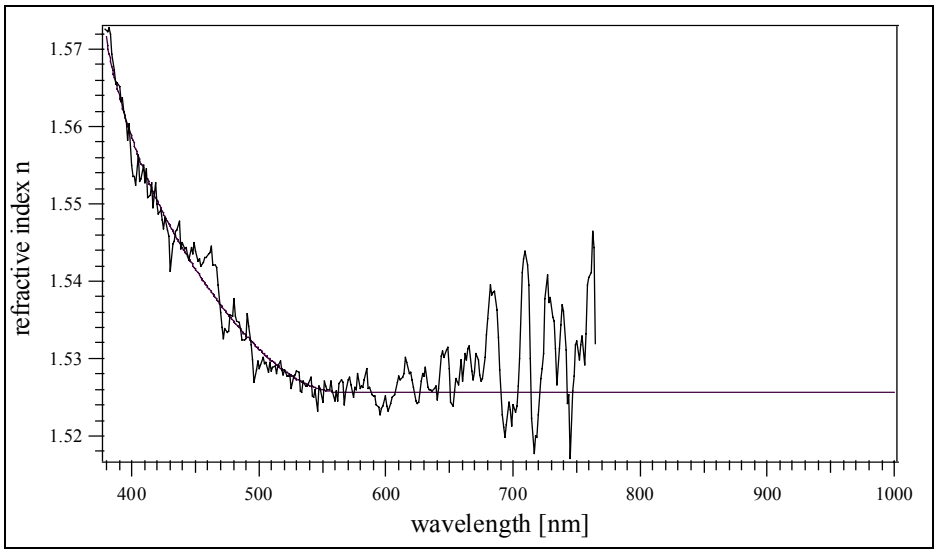

Figure 3.2: Dispersion relation of the glass substrate inferred from the measured transmission spectrum displayed in Fig. 3.1 by using equations 3.2 and 3.4. A smoothed curve has been generated and added to the figure.

3.2 Method based on Positions of Maxima and Minima

This method is applicable when a measured transmission spectrum exhibits certain oscillations in the region of transparency, and it works well even in the case of extremely small amplitudes (refractive index of the film close to the one of the substrate). As an example, Fig. 3.3 shows experimental transmittance spectra for a set of films deposited in the sol-gel dip-coating process varying the withdrawal speed. The origin of the oscillations is related to constructive and destructive thin film interference and maxima/minima occur for integer multiples of quarter wave layers [KNI76].

One condition for the occurrence of such oscillations is the requirement that the thickness exceeds a certain value. From an analysis of these oscillations, both the refractive index n and the optical film thickness n*d can be inferred directly from the measured spectra.

The method described in the following is especially suitable to characterize the optical properties of SiO_2 films.

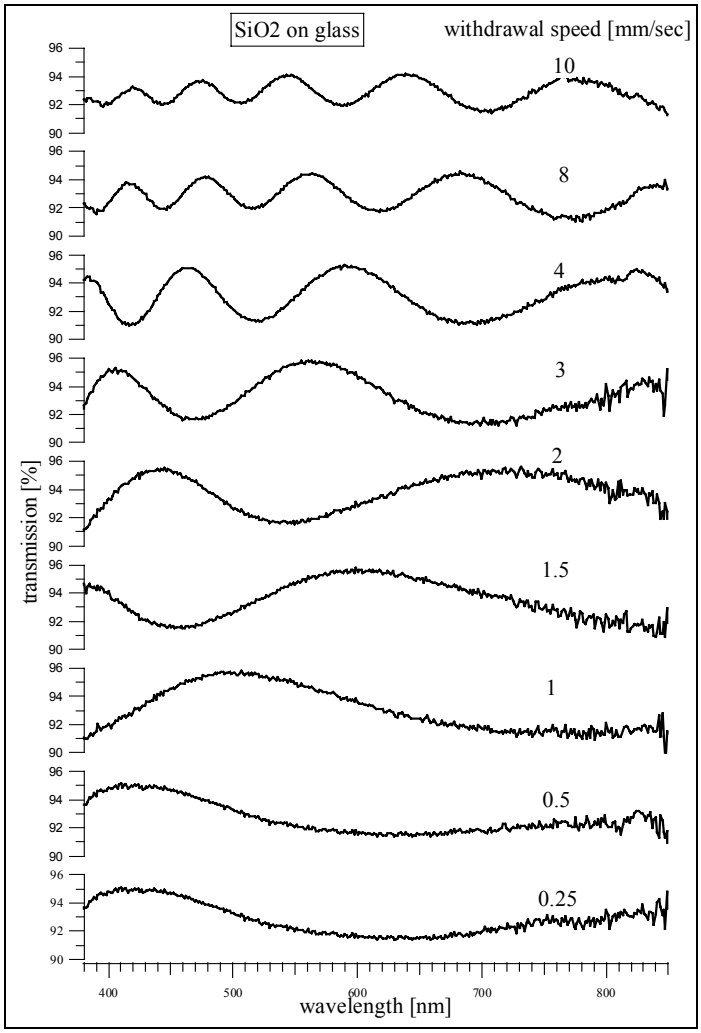

Figure 3.3: Transmission of a set of SiO_2 films on glass deposited at different withdrawal speeds and therefore of different thicknesses. Oscillations resulting from destructive and constructive interference are clearly visible.

3.2.2 Direct Determination of the Refractive Index n

For special wavelengths, the refractive index n can be directly inferred from the amplitude of the oscillation in the transmittance or reflectance spectra. The theoretical relation of the double of the amplitude of oscillation (in the figure denoted as delta R) to the difference in refractive index (delta n) between substrate and film is illustrated in Fig. 3.4. The spectra oscillate between the value of the uncoated substrate and a value dependent on the difference of the refractive indices. The positions where the transmittance and reflectance equal the one of an uncoated substrate correspond to integer multiples of halfwave layers (“absentee layers”). A value of the difference in refractive indices can thus be inferred directly for each position of either the reflection minima respectively the transmission maxima (in the case of n inferior for film than for substrate) or for each position of the reflection maxima respectively the transmission minima (in the case of n larger for the film than for the substrate). At those special wavelengths we obtain thus directly precise values for the refractive index n reflecting the dispersion relation of the material. The results for silicon dioxide are shown in Fig. 3.5. The data can be interpolated by a numerical fitting a Cauchy dispersion formula.

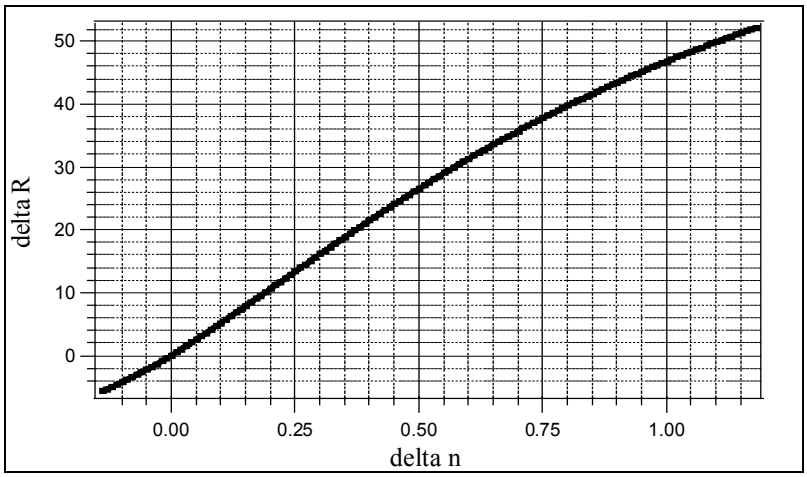

Figure 3.4: Relation of the double (delta R) of the amplitude of oscillation to the difference in refractive indices of film and substrate.

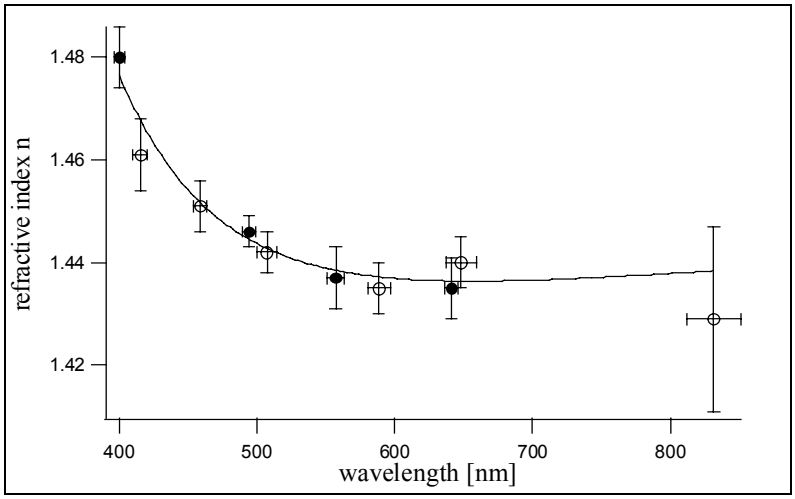

Figure 3.5: SiO_2 film dispersion relation obtained by using oscillating transmittance spectra and the relation plotted in Fig. 3.4. The data have been interpolated by numerically fitting a Cauchy dispersion formula.

3.2.1 Determination of d for Slowly Varying Refractive Index

In the case of an approximately constant index of refraction n (dispersion small), a good estimate for the film thickness can be inferred directly.

When the refractive index of the film is inferior than the one of the substrate, maxima in the reflection (minima in transmission) can usually be observed at the following wavelengths:

$\lambda = \lambda_0/2, \lambda_0/4, \lambda_0/6, \lambda_0/8, \ldots, \lambda_0/2m$ with m = 1, 2, 3, …

while minima in reflectance (maxima in transmission) occur at the following wavelengths:

$\lambda = \lambda_0, \lambda_0/3, \lambda_0/5, \lambda_0/7, \ldots, \lambda_0/(2m+1)$ with m = 1, 2, 3, …

where $\lambda_0 = 4nd$ (n assumed to be constant).

In the general case extrema are found at:

$$\lambda j = \lambda_0/j \qquad \textbf{Equation 3.1}$$

with j = 1, 2, 3, … (See example in Fig. 3.3)

This expression can be rearranged to yield:

$$\frac{1}{\lambda_j} = \frac{1}{\lambda_0} \cdot j \qquad \textbf{Equation 3.2}$$

By reading the extrema positions from the spectrum and plotting $1/\lambda_j$ against j, the value $1/\lambda_0$ is identified as the slope s, of the graph, hence

$$n \cdot d = \frac{1}{4 \cdot s} \qquad \textbf{Equation 3.3}$$

An example of such an analysis is given in Figs. 3.6 and 3.7, based on the measurements shown in Fig. 3.3. The linearity of the graph illustrated by Fig. 3.6 confirms that the index of refraction of the SiO_2 layer is nearly constant. Assuming a value of n = 1.47 the film thicknesses presented in Fig. 3.7 are found.

3.2.1 Determination of d in the General Case

When the refractive index varies considerably with the wavelength, the plot of extrema positions will no longer be linear. In this case it is preferable to determine the film thickness by a numerical fit using a software as e.g. Tfcalc. Given the dispersion relation for n, one spectrum of transmission or reflection is usually sufficient to extract the desired information on the film

thickness accurately. Care has to be taken not to trust the wrong local minimum of the least square error. It might be helpful to use the plot of the extrema positions in order to obtain a rough estimate of the film thickness before determining it precisely by the numerical fit.

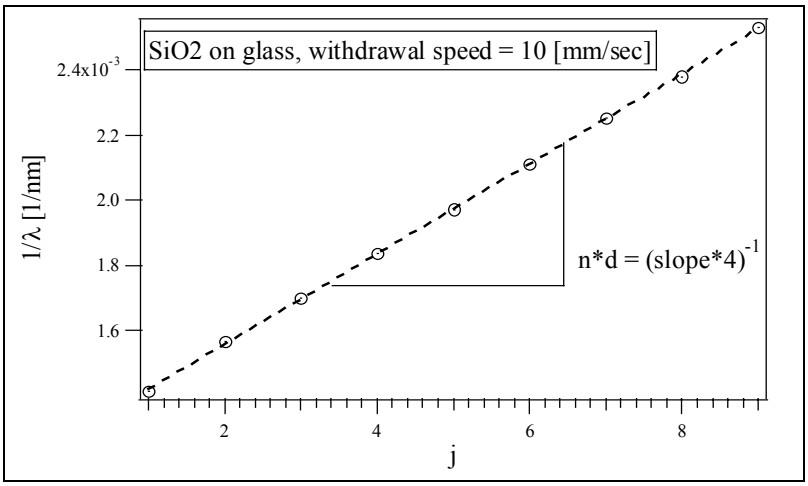

Figure 3.6: Positions of maxima and minima in the transmission spectra of a SiO_2 film are plotted vs. the number of order j . The graph exhibits nearly perfect linear behavior. The slope of the plot gives a value for the optical path nd.

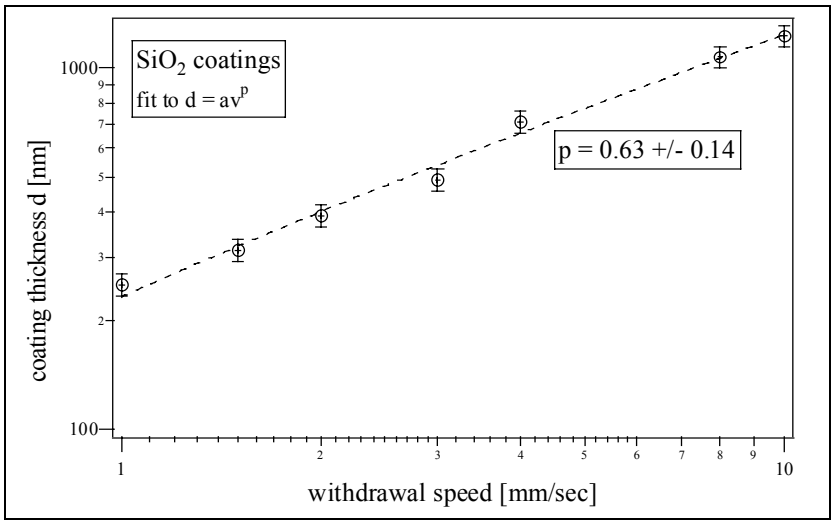

Figure 3.7: Approximated thickness of SiO_2 layers using the maxima and minima positions method. N is assumed to be constant, equal to 1.47. The power law compares to the Landau-Levich relation, predicting an exponent value of 2/3, where d is the layer thickness, v the withdrawal speed, and a is a constant depending of the solution used for the deposition [LAN42].

3.3 Method based on Angular-Dependent Measurements

In the absence of oscillations (e.g. in the case of thinner films) the method of maxima/minima values and positions described in section 3.2 is not applicable. In this case, a set of transmittance/reflectance spectra has to be measured for various angles of incidence. Special software (e.g. the program “Tfcalc”) is employed for the data analysis by a least square fit.

3.3.1 Software for Simulation of Thin Films Coatings

The software TFCalc is a suitable tool for the design of interference filters. It allows to simulate and optimise the optical behaviour of multi-layered thin film stacks. The numerical calculations are based on the characteristic matrices. The optical properties of each layer can be represented by a 2x2 matrix and the multilayered stack described by their matrix product.

In TFCalc the user defines the thin film stack and its environment: the refractive index n(λ), the extinction coefficient k(λ) for the substrate and the thin film materials; the stacking of thin films on the substrate and thicknesses of individual layers; the illuminant incident on the film and a detector embedded in the exit medium.

As well as the simulation of transmittance and reflectance spectra, TFCalc allows a determination of the parameters n, k and d for a given set of input data. Due to the nature of the program, this procedure has to be performed for each wavelength separately.

3.3.2 Point-by-Point Analysis of Angle-Dependent Spectra

A set of transmittance/reflectance spectra is acquired from the considered thin film sample. In the region of transparency a set of transmittance spectra is sufficient, because in this case the reflectance spectra do not contain additional information. An example for titanium dioxide on glass is shown by Fig. 3.8.

The refractive index of the substrate is determined (see section 3.1.3) and imported into the software.

For selected wavelengths, the angle-dependent transmittance or reflectance data are extracted from the full spectra (see Fig. 3.9) and imported into the software as target values. In the case of a substrate coated symmetrically on both sides, the problem can be simplified to the one of a single coated surface according to section 3.1.2.

The function “optimize” can be now used to determine n, k and d for each wavelength separately. In the region of transparency, k is set to zero. The film thickness d has to be the same for all wavelengths, which allows a cross-check of the results. Fig. 3.10 illustrates the result for the refractive index n of titanium dioxid on glass, as obtained from the data shown in Figs. 3.8 and 3.9. The obtained values for n have been interpolated by fitting a Cauchy dispersion formula to the data.

Transmittance and reflectance measurements can be made using polarisation filters which separate the incident light into s- and p-polarised components. This option yields for a given wavelength more data targets for the optimisation, thus enhancing the precision and the certainty of the method.

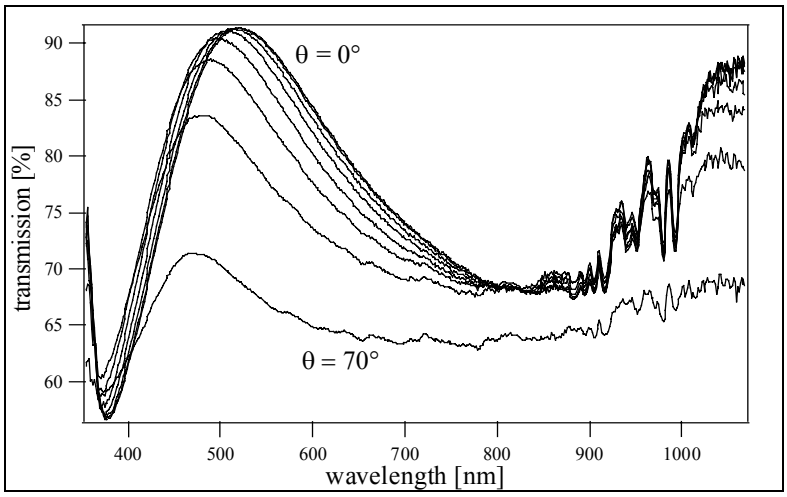

Figure 3.8: Transmission spectra for a range of incident angles for a double side coated TiO_2 thin film on glass.

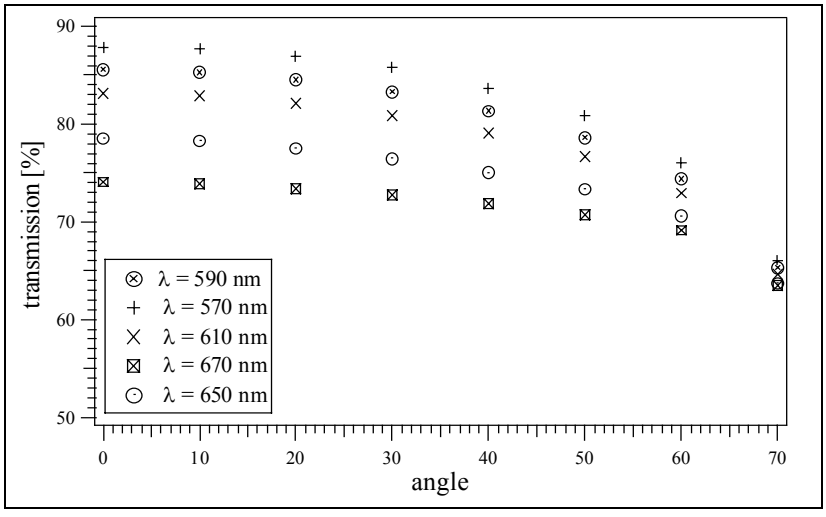

Figure 3.9: Transmission values versus angle for a selection of different wavelengths. Each data set is imported into the simulation software TFCalc as target values for the determination of the parameters n, k and d.

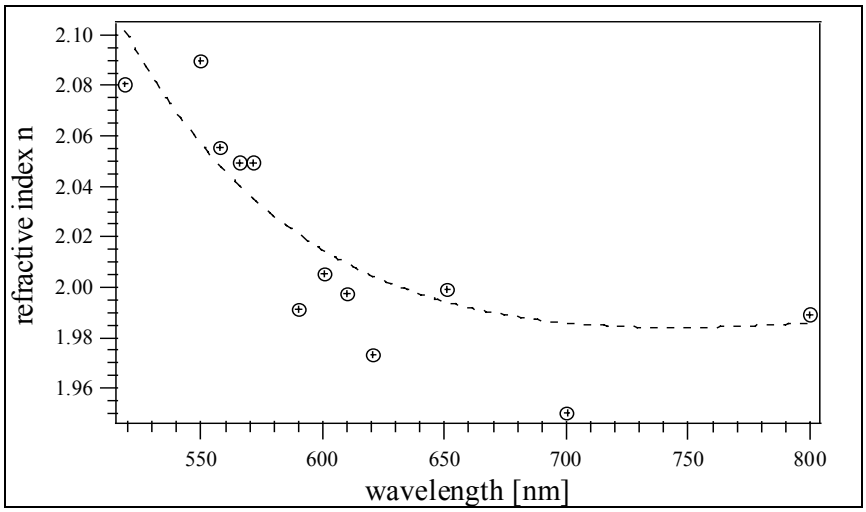

Figure 3.10: Dispersion relation for TiO2 thin film inferred from the angle dependent behaviour of transmitted light (Figs. 3.8 and 3.9). The dashed line represents a Cauchy dispersion relation fitted to the data.

REFERENCES

[KNI76] Z. Knittl, *Optics of Thin Films*, Wiley, London (1976)

[LAN42] L.D. Landau, B.G. Levich, Acta Physiochim. 17 (1942) 42 (U.R.S.S)

4 Colorimetry

4.1 Definitions

In order to make statements about achieved colors, color saturation, angle dependence of colors, color stability etc., a quantitative way of describing color is extremely important for any work on colored solar collectors. The International Commission on Illumination (CIE, Commission Internationale d'Eclairage) described how to quantify colors [CIE86, SEV96]. All existing colors can be represented in a plane and mapped by Cartesian coordinates, as shown in the CIE Chromaticity Diagrams. The quantification is based on the 1931 CIE Color Matching Functions, $x(\lambda)$, $y(\lambda)$, and $z(\lambda)$, which reflect the color sensitivity of the human eye. These functions depend to some extent on the width of the observation field (functions given for an opening angle of 2° and 10°). Tristimulus values X, Y, and Z are computed from three similar integrations of the measured or simulated spectral power distribution data $P(\lambda)$:

$$X = \int P(\lambda) \cdot x(\lambda) d\lambda$$
$$Y = \int P(\lambda) \cdot y(\lambda) d\lambda \qquad \textbf{Equation 4.1}$$
$$Z = \int P(\lambda) \cdot z(\lambda) d\lambda$$

The spectral power distribution $P(\lambda)$ can be, for example, the product of a source spectrum and a simulated or measured reflection spectrum. In the case of Lambertian or specular reflecting surfaces, one can work with the hemispherical reflectance $R(\lambda)$. Representing typical daylight, the standard illuminant D_{65} is commonly used as source:

$$P(\lambda) = D_{65}(\lambda) \cdot R(\lambda) \qquad \textbf{Equation 4.2}$$

From these tristimulus values, the 1931 CIE color coordinates x, y, z are defined as:

$$x = X/(X+Y+Z)$$
$$y = Y/(X+Y+Z) \qquad \textbf{Equation 4.3}$$
$$z = 1-(x+y)$$

All existing colors are represented in the x, y plane, as illustrated by Fig. 4.1.

In order to represent color differences more realistically, the CIE introduced in 1976 the u',v' color space. These color coordinates u', v' can be derived from the tristimulus values directly, too:

$$u' = 4X/(X+15Y+3Z)$$
$$v' = 9Y/(X+15Y+3Z) \qquad \textbf{Equation 4.4}$$

Alternatively, they can be computed by conversion of the 1931 coordinates:

$$u' = 4x/(-2x + 12y + 3)$$
$$v' = 9y/(-2x + 12y + 3)$$

Equation 4.5

Fig.4.2 visualizes the u', v' color space.

Another transformed color coordinate system is the CIELAB color space defined by L*, a* and b* :

$$L^* = f(Y/Y_n)$$

$$a^* = \frac{500}{116}\left[f(Y/Y_n) - f(Y/Y_n)\right]$$

Equation 4.6

$$b^* = \frac{200}{116}\left[f(Y/Y_n) - f(Z/Z_n)\right]$$

where

$$f(R) = 116R^{1/3} - 16 \quad \text{if } f(R) \geq 8$$

and

$$f(R) = (29/3)^3 R \quad \text{if } f(R) < 8$$

X_n, Y_n and Z_n are the tristimulus values of the reference illuminant (e.g. for D_{65}: X_n = 95.04, Y_n = 100, Z_n = 108.88).

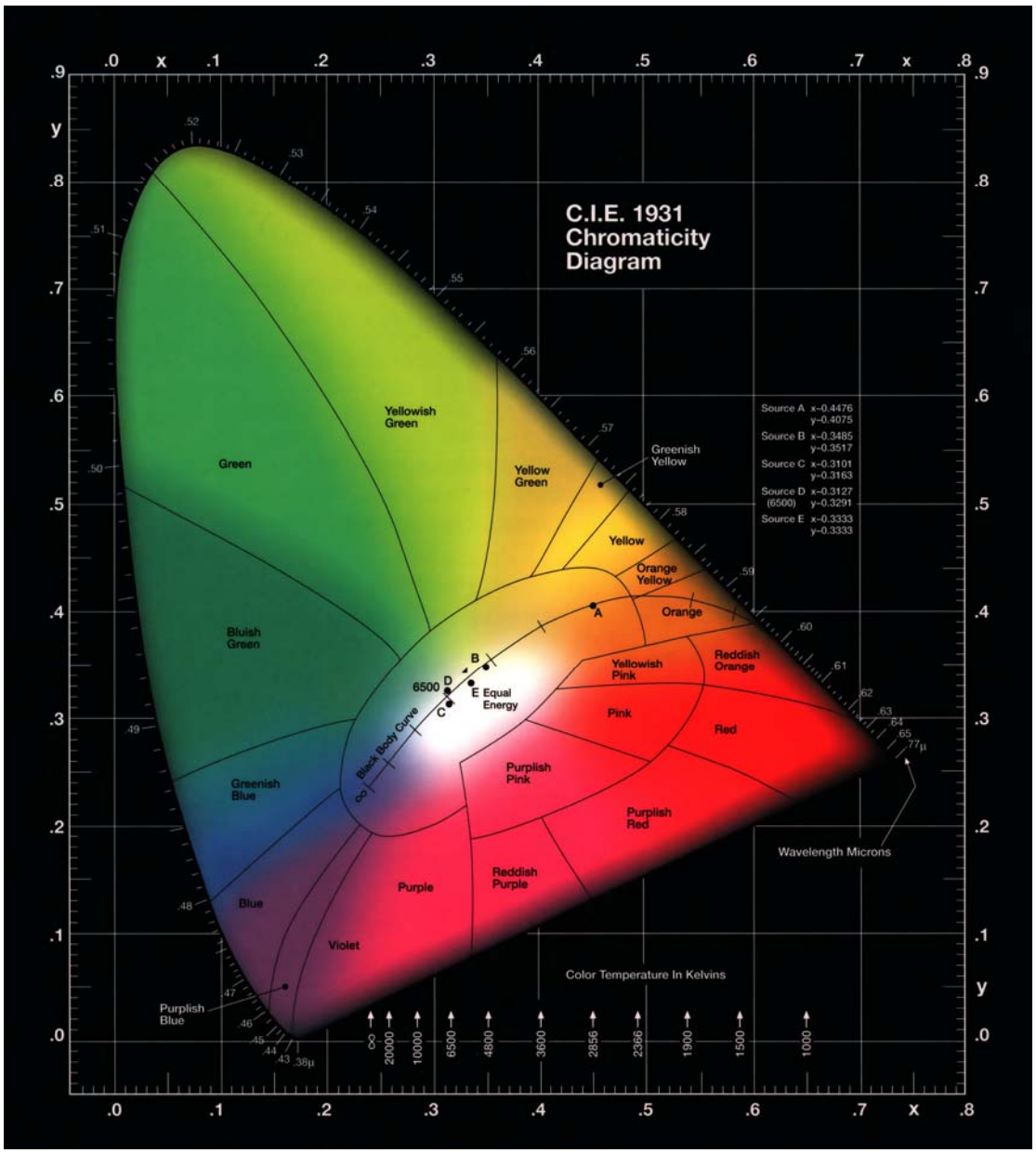

Figure 4.1: CIE x, y color space (1931).

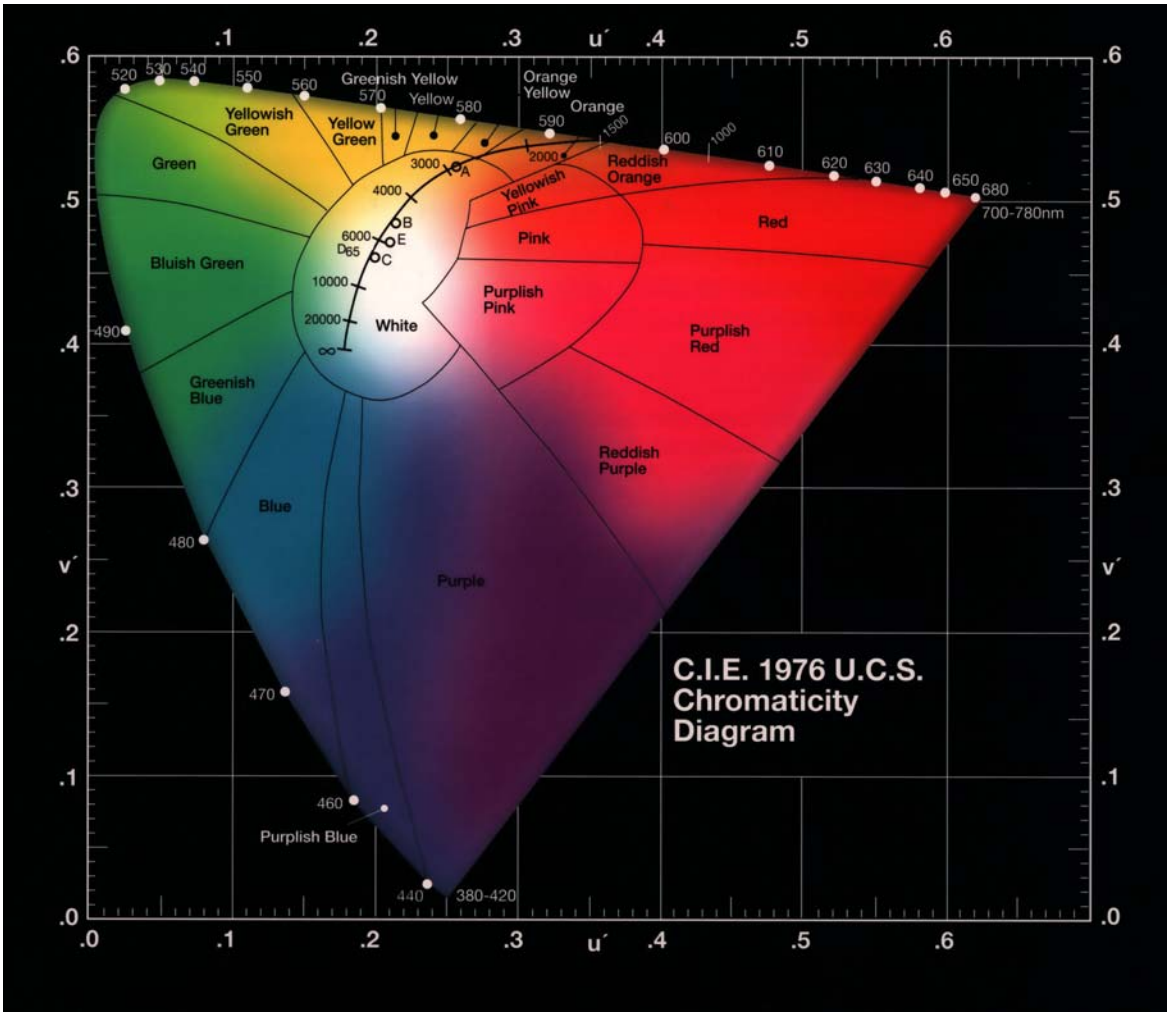

Figure 4.2: CIE u', v' color space (1976).

4.2 Comparison of Methods

A set of four reference samples has been investigated by two different methods, with a hand-held device based on a flash and three sensors, and by acquiring spectra of the total hemispherical reflectance by means of the spectrometer described in Chapter 2 in combination with the integrating sphere. The CIE color coordinates x, y and Y have been obtained from the reflectance spectra by the formulae described above.

hand-held device:
MINOLTA Cr-210b

spectrophotometer:
MultiSpec 125^{TM} 1/8m, Oriel, with INSTASPEC II^{TM} detector head and integrating sphere

reference samples:
Labsphere reflectance standards

SCS-R-020	(red)
SCS-B-020	(blue)
SCS-G-020	(green)
SCS-Y-020	(yellow)

A Data sheet with the corresponding CIE color coordinates has been provided by the manufacturer (calibration certificate based on NIST standards).

Fig. 4.3 shows a comparison of the results for the CIE color coordinates x, y and Y as determined by the different methods (for an opening angle of 2° and the standard illuminant D_{65}). While there are no two methods agreeing perfectly, there is not any method yielding completely different results. The differences give an idea about the precision of this type of measurements. For the numerical results see table 4.1. The standard deviation has been computed for each color coordinate and each sample, and a mean value of the standard deviation for each coordinate averaged over all samples.

The precision is thus estimated to be in the order of +/- 0.005 for x and y (+/- 0.04 and +/- 0.06, respectively, see table 4.1), and in the order of +/- 1.6 for Y.

Within this error range, the x, y and Y values obtained by the spectrophotometer have thus been confirmed by as well the reference values from the sample manufacturer as the values directly measured using the instrument MINOLTA Cr-210b.

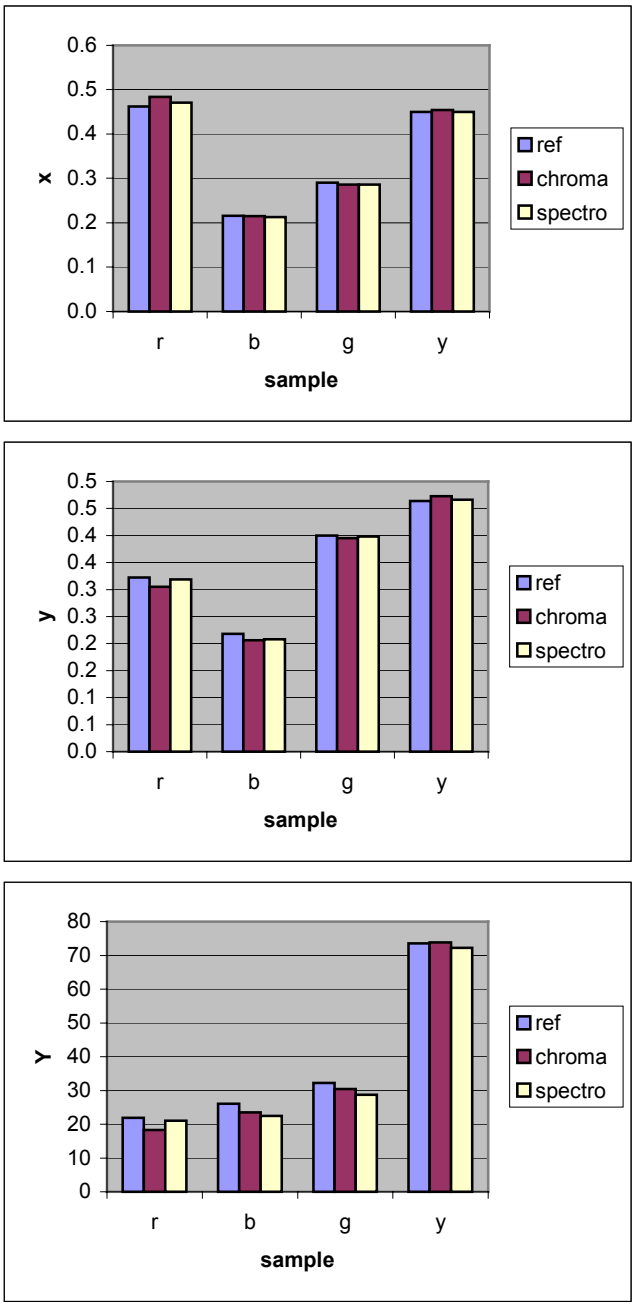

Figure 4.3: CIE color coordinates x, y and Y, as determined for four reference samples (colors red, blue, green and yellow, denoted as r, b, g, y) by the Minolta instrument (chroma) and by the spectrophotometer with integrating sphere (spectro). The measured values are compared to the reference values provided by the manufacturer of the reference samples (ref). The differences give an idea about the precision of this type of measurements. While there are no two methods agreeing perfectly, there is not any method yielding completely different results.

CIE coord	sample	ref	chroma	spectro	mean	+/-	mean +/-
x	r	0.462	0.484	0.471	0.472	0.011	
	b	0.216	0.215	0.213	0.215	0.002	
	g	0.290	0.286	0.286	0.287	0.002	
	y	0.450	0.454	0.450	0.451	0.002	0.004
y	r	0.322	0.305	0.319	0.315	0.009	
	b	0.218	0.206	0.208	0.211	0.006	
	g	0.400	0.395	0.398	0.398	0.003	
	y	0.464	0.473	0.466	0.468	0.005	0.006
Y	r	21.9	18.3	21.0	20.4	1.9	
	b	26.1	23.5	22.5	24.0	1.9	
	g	32.2	30.4	28.7	30.4	1.8	
	y	73.6	73.8	72.2	73.2	0.9	1.6

Table 4.1: CIE color coordinates x, y and Y, as determined for four reference samples (colors red, blue, green and yellow, denoted as "r", "b", "g", "y") by the Minolta instrument ("chroma") and by the spectrophotometer with integrating sphere ("spectro"). The measured values are compared to the reference values provided by the manufacturer of the reference samples ("ref"). The standard deviation ("+/-") is given for each color coordinate and each sample, and a mean value of the standard deviation for each coordinate averaged over all samples.

REFERENCES

[CIE86] International Commission on Illumination CIE, *Colorimetry*, CIE Publication 15.2., 2nd Ed., ISBN 3-900-734-00-3, Vienna, (1986)

[SEV96] R. Sève, *Physique de la Couleur*, Masson, Paris (1996)

5 Solar Simulator and Power Measurements

For any solar collector glazing, a sufficiently high solar transmittance is an essential requirement. In this chapter we present a method for a direct measurement of the solar transmittance, based on a solar simulator and a thermopile detector with a constant spectral sensitivity. For terrestrial applications, the global solar spectrum at air mass 1.5 ("AM1.5g") is one of the most common choices as reference for the illuminant. Special filters are used to match the spectrum of the source to the desired solar spectrum.

5.1 Solar Simulator - Technical Data

Universal arc lamp housing: Oriel 66902, 50-500W

Lamp: 150 Watt ozone free Xenon arc lamp

Power supply: Oriel, Arc Lamp Power Supply.

Filters: Oriel, models 81090, 81092, 81091, 81094

5.2 Source and Filters

The Oriel Solar Simulator contains a Xenon arc lamp providing a close match to the solar spectrum. Though the match is not exact it is close enough for many applications. The xenon arc lamp emits a 5800 K blackbody-like spectrum, which is very close of the real sun's spectrum, with the addition of line structure. The lamp housing contains a condensor producing a collimated beam.

The purpose of filters used on the collimated beam is to re-shape the spectral output.

Within the spectral range from 800 to 1000 nm the xenon lamp exhibits unwanted spectral lines. The filter model 81090 is used to reduce the mismatch and approximate the Air Mass 0 radiation. Combinations of different filters (giving approximation of Air Mass 1.5 direct and global radiations) also modify the visible and ultraviolet portion of the spectrum for a better match to the standard solar spectra.

Filter combination 1 : filters 81090, 81091 and 81094

Filter combination 2 : filters 81090 and 81092

5.3 Radiant Power Energy Meter

The Oriel 70260 is a microprocessor-based Radiant Power/Energy Meter providing a wide range of measurements. The most sensitive thermopile detector available has been chosen for our experiments.

5.3.1 Technical Data

Radiant Power Meter, Oriel, model 70260

Thermopile Probe, Oriel, model 70264

Fused silica filter for the thermopile 70264, Oriel, model 44950

5.3.2 Thermopile Absorber Head and Fused Silica Filter

The thermopile consists of thermocouple junctions linked in series. When a radiant heat source, such as a light source or laser, is directed at the absorber head aperture, a temperature gradiant is created across the thermopile of the enclosed detector disc. This generates a voltage proportional to the incident power. The display unit amplifies this signal and indicates the power level received by the head. At the same time, signal processing software causes the display unit to respond faster than the thermal rise time of the detector disc, thus reducing the response time of the Radiant Meter. Energy of a single pulse is measured by integrating the pulse power over time.

The 70264 head has a spectral range of 190 nm to 2000 nm, a power measurement range of 2 mW to 10 W and an energy measurement range of 3 μJ to 10 J.

Used with the thermopile probe, a fused silica filter absorbs radiation above 3 μm, allowing more sensitive measurements in the UV to NIR.

Combining the solar simulator and power measurements, solar transmission factors can be measured as shown in Table 5.1.

Filter combination 2 seems to be most suitable for the application. The deviations from the spectrophotometric values amount only to approx. 1 % .

Sample	Spectrometer Basel Varian CARY 5 Transmission [%]	Solar simulator Filter combination 1 Transmission [%]	Solar Simulator Filter combination 2 Transmission [%]
A	92	92	91
B	89	87	88
C	87	85	86
D	90	90	89
E	85	82	84
F	82	81	82

Table 5.1 : Solar transmission factors for multilayered sputtered thin films samples (A to F) obtained by different methods. Spectrophotometric measurements have been performed at the University of Basel using the instrument Varian CARY 5 . The adjacent columns show values obtained by the solar simulator in combination with the radiation power meter using different filter combinations.

6 Spectroscopic Ellipsometry

6.1 Description

Spectroscopic ellipsometry is a precise optical measurement technique working with polarized light. The method compares the ratio of the reflection coefficients for parallel and perpendicular polarized light R_p and R_s . This relative measurement makes the technique independent from intensity fluctuations of the source, thus favoring a high precision. Output of the experiment are the ellipsometric angles Ψ and Δ , defined by the equation:

$$\tan(\psi)\exp(i\Delta)=\frac{R_p}{R_s} \qquad \textbf{Equation 6.1}$$

A scheme of the experimental configuration is shown in Fig. 6.1. Linearly polarized light is incident on the sample (components parallel and perpendicular to the plane of incidence both non-zero). After reflection the polarisation will be in general elliptical, which is characterized by a detector behind a rotating analyzer, eventually in combination with a retarder (not shown in Fig 6.1). In spectroscopic ellipsometry, the use of a grating monochromator allows the acquisition of wavelength-dependent data.

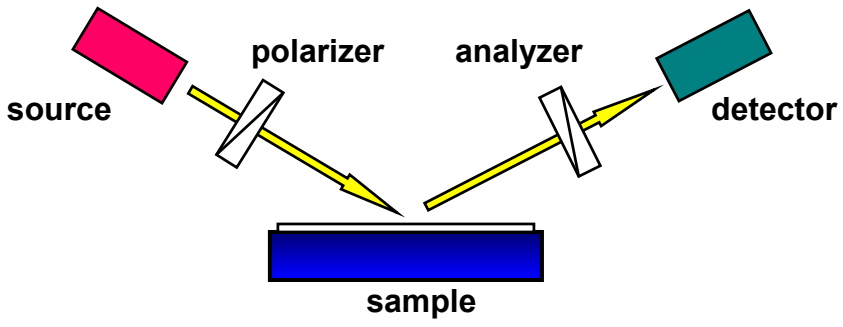

Figure 6.1: Scheme of ellipsometric measurements. After reflection of originally linearly polarized light the polarisation will be in the general elliptical, which is characterized by a rotating analyzer and a detector, eventually in combination with a retarder (not shown in the figure).

6.2 Analysis of Experimental Data

In order to infer the optical constants *n* and *k* and the thickness of thin film samples from the acquired spectra of Ψ and Δ, commonly a function for the dispersion relation is assumed, for example a Cauchy dispersion relation:

$$n(\lambda) = n_0 + C_0 \frac{n_1}{\lambda^2} + C_1 \frac{n_2}{\lambda^4} \qquad \textbf{Equation 6.2}$$

and

$$n(\lambda) = n_0 + C_0 \frac{n_1}{\lambda^2} + C_1 \frac{n_2}{\lambda^4} \qquad \textbf{Equation 6.3}$$

with the wavelength λ and the constants n_i, k_i, $C_0 = 10^2$ and $C_1 = 10^7$. The numbers n_i, k_i, can be used together with the film thickness *d* as parameters of a numerical fit to the experimental data.

As an example we consider a thin film of SiO_2 deposited by reactive magnetron sputtering on a silicon wafer (see ref. [SCH03]). The ellipsometric angles psi and delta have been measured for various angles of reflection (40°, 50°, 60°, and 70°) by means of an ellipsometer SENTECH SE 850 (group of Prof. Oelhafen, University of Basel). The experimental results are displayed in Fig. 6.2. These data are analysed on the basis of an optical model, where the optical properties of the individual thin film are assumed to follow a Cauchy dispersion relation. The numerical fitting procedure yields the function $n(\lambda)$ shown in Fig. 6.3, the extinction coefficient *k* close to zero (within the considered wavelength range), and a film thickness of 154 nm. Spectroscopic ellipsometry is even applicable to multilayered samples [BOU03].

In preliminary experiments it could already be shown that the method is also working for samples produced at LESO by the sol-gel dip-coating process and measured at the University of Basel. Eventually, additional ellipsometric measurements might be performed in collaboration with the group of Prof. Lévy at EPFL (instrument UVISEL, Jobin-Yvon).

REFERENCES

[SCH03] A. Schüler, C. Roecker, J.-L. Scartezzini, J. Boudaden, I. R. Videnovic, R. S.-C. Ho, P. Oelhafen, *Interference filters for colored glazed thermal solar collectors,* Proceedings of ISES World 2003 Conference, 14-20 June 2003, Göteborg (Sweden).

[BOU03] J. Boudaden, R. S-C. Ho, P. Oelhafen, A. Schüler, C. Roecker, J.-L. Scartezzini, *Towards colored glazed thermal solar collectors,* Proceedings of ISES World 2003 Conference, 14-20 June 2003, Göteborg (Sweden)

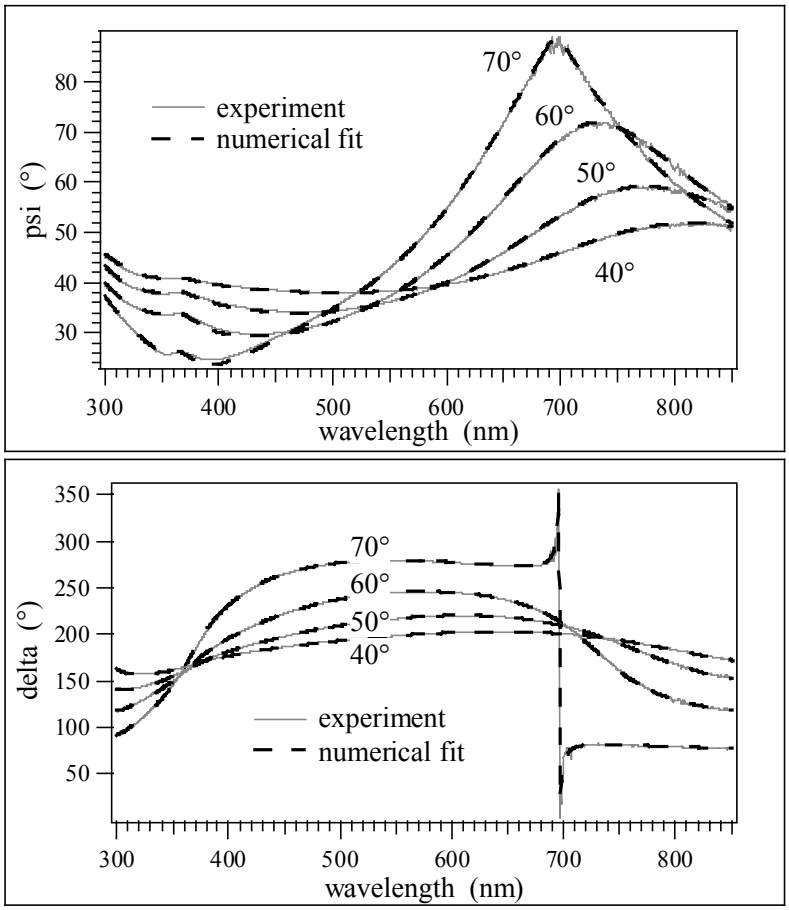

Figure 6.1: Spectroscopic ellipsometry of a sputtered SiO_2 film on a silicon substrate. The experimental data on the ellipsometric angles psi and delta have been fitted assuming a Cauchy dispersion relation (data from ref. [SCH03]).

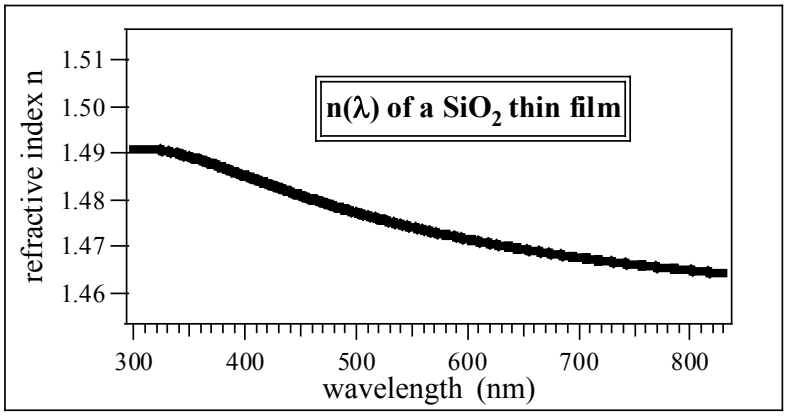

Figure 6.2: The refractive index n(λ), as inferred by numerical analysis of the ellipsometric data shown in Fig. 6.1. An extinction coefficient k of zero (within the considered wavelength range), and a film thickness of 154 nm have been found.

7 Scanning Electron Microscopy

In order to optimize coating durability, it is essential to obtain information on the film morphology, which comprises film properties such as crystallite sizes and the type of film growth (e.g. columnar, cauliflower or compact). Electron microscopy of aged samples indicates in many cases the dominant aging mechanism such as adhesion failure or diffusion processes. Scanning electron microscopy will give insight into the nature of the coating defects (due to e.g. dust particles from air or crystallites from solution), and will thus help to achieve the goal of high quality coatings exhibiting only few defects. Additionally, for the interpretation of optical measurements, it is very helpful to simply "take a look" at the thin film by electron microscopy, thus checking the optically determined film thickness, the presence of voids and the roughness of surface and interfaces. From cross-sectional electron micrographs, the film morphology becomes often directly apparent. In many cases the crystallite size and even some indications of the texture (preferential orientation of the crystallites) can be inferred. For this type of measurements, thin films are prepared on specially prepared silicon substrates (groove at back side), and then broken carefully. Top and cross-sectional views can then be acquired in the electron microscope. By the use of a conducting Si substrate, charging effects are kept to a tolerable level.

An example is shown in Fig. 7.1 (data from ref. [SCH01a]). A titanium aluminum nitride thin film ($Ti_{0.62}Al_{0.28}N$) has been deposited on a silicon wafer by reactive magnetron sputtering. The sample has been investigated by means of a JEOL 6300F scanning electron microscope (Laboratory of Scanning Electron Microscopy, University of Basel). In the top view, an agglomeration of little pyramids is observed, with their basis triangular and the edges in the order of 30 nm [Fig. 7.1a)]. The side view shows a columnar film growth with column diameters in the order of 30 nm, revealing that the pyramids are the upper termination of the columns [Fig 7.1b)]. This needle-like morphology may be accompanied by a preferential orientation of the crystallites (texture).

Within this project, scanning electron microscopic investigations are foreseen in collaboration with the Interdepartmental Center of Electron Microscopy at EPFL (Prof. Buffat). Individual and multilayered thin films will be prepared on specially prepared silicon substrates. The method of sol-gel thin film deposition on backside-grooved silicon substrates has already been checked.

REFERENCES

[SCH01a] A. Schüler, V. Thommen, P.Reimann, P. Oelhafen, G. Francz, T. Zehnder, M. Düggelin, D. Mathys, R. Guggenheim, *Structural and optical properties of titanium aluminum nitride films ($Ti_{1-x}Al_xN$)*, J. Vac. Sci. Technol. A 19 (2001)

a)

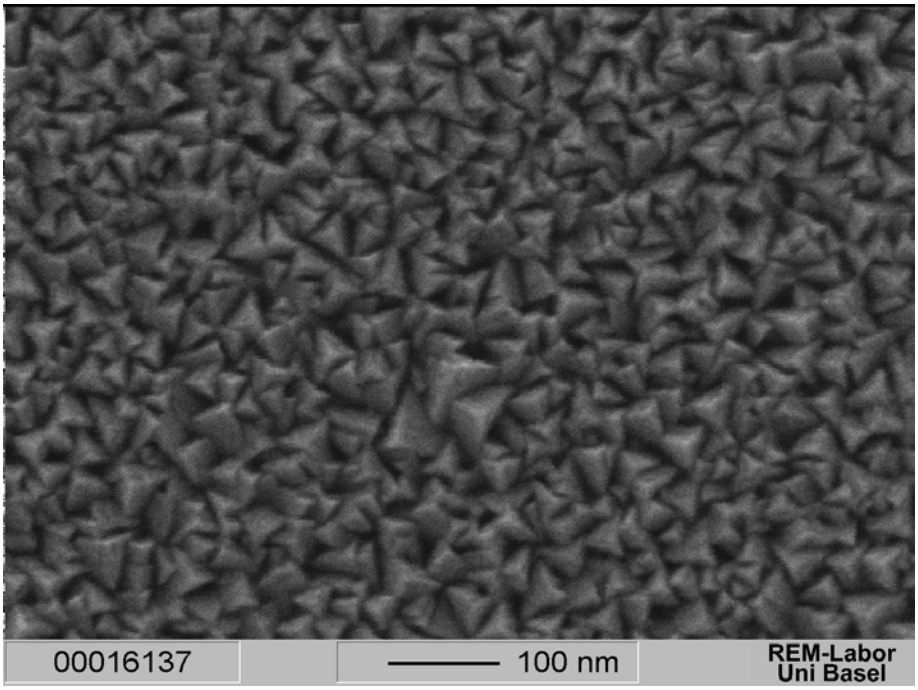

b)

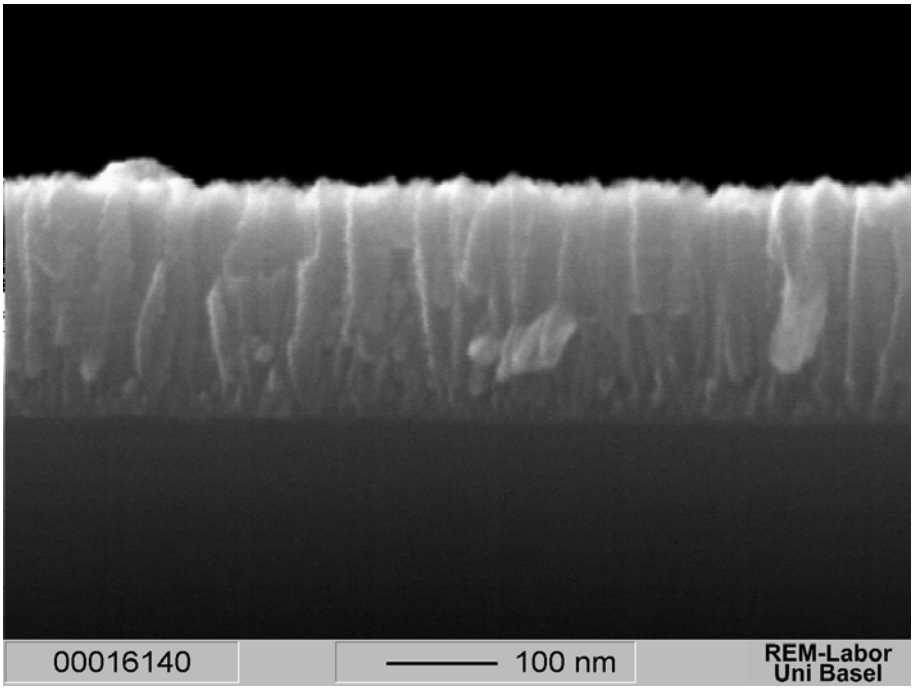

Figure 7.1: Scanning electron microscopy of a titanium aluminum nitrid film ($Ti_{0.62}Al_{0.38}N$) deposited on a silicon substrate by reactive magnetron sputtering (from reference [SCH01a].

a) In the top view little pyramids are distinguished. The facettes reflect the crystalline nature of the films.

b) The side view of the edge of a breaking reveals that the pyramids observed in the top view are related to a columnar film structure, with column widths in the order of 30 nm. The total film thickness amounts to approx. 230 nm.

8 X-ray Diffraction (XRD)

8.1 Description

When optimizing aging properties of thin films, the identification of crystalline phases, the crystallite size, and the eventual preferential orientation of the crystals (texture) are valuable information. X-ray diffraction is a powerful tool to investigate the mentioned properties. Measurements on thin films are performed in a diffractometer preferably under grazing incidence, thus enhancing the signal to noise ratio. The commonly chosen geometry is depicted in Fig. 8.1. 2θ designates the angle between incident and diffracted beams, while Ω represents the (small) incidence angle.

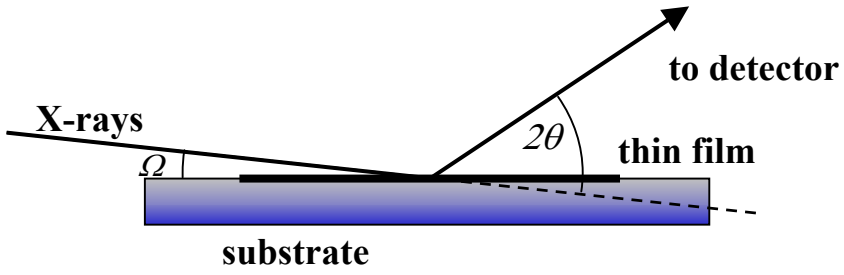

Figure 8.1: Geometry of X-ray diffraction experiments. 2θ designates the angle between incident and diffracted beams, while Ω represents the incidence angle.

8.2 Data interpretation

Peak positions and intensities for many materials can be found in databases of powder diffraction files such as that of the Joint Committee on Powder Diffraction Standards (JCPDS) (see [JCPDS]). From the occurence of the diffraction peaks in the experimental diffraction patterns, crystalline phases can thus be identified.

The width of the peaks results from the combined effects of the crystallite size, internal strain, pointdefects, and of the instrumental broadening.

Assuming that the influence due to strain and point defects is weak, the grain size d_{grain} can be calculated according to the Scherrer formula (e.g. ref. [CUL78]).

$$d_{grain} = \frac{0.9\lambda}{B_{grain}\cos(\alpha)} \qquad \textbf{Equation 8.1}$$

where B_{grain} is obtained from the measured peak width B_{meas}

$$B_{meas}^{\ 2} = B_{instr}^{\ 2} + B_{grain}^{\ 2} \qquad \textbf{Equation 8.2}$$

An example is shown in Fig. 8.2 (from [SCH01a]). All the peaks occuring in the diffraction pattern can be identified to be due to one single phase, the substitutional solid solution (Ti, Al)N of the cubic NaCl - type structure. The dashed lines indicate the peak positions for the cubic TiN. For the solid solution (Ti,Al)N the diffraction peaks are shifted towards the large angle side. This is due to a shrinkage of the lattice parameter caused by the substitution of Ti atoms by the smaller Al atoms. The (200) peak, being the most intense one for TiN, is nearly completely missing for the $Ti_{0.62}Al_{0.38}N$ sample, indicating some preferential orientation of the individual grains. For the observed linewidths, the Scherrer formula yields a lower limit for the grain size of 10 nm.

Within this project, measurements of X-ray diffraction are envisaged in collaboration with the group of Prof. Lévy at EPFL. The contact has been established and will allow us the access to the X-ray diffractometer.

REFERENCES

[JCPDS] *PDF-database.* JCPDS, International center for diffraction data (ICDD), 1601 Park Lane, Swarthmore, PA 19081, USA

[CUL78] B.D. Cullity, *Elements of X-ray diffraction*, 2nd Ed., Addison-Wesley Publishing Company Inc. (1978)

[SCH01a] A. Schüler, V. Thommen, P.Reimann, P. Oelhafen, G. Francz, T. Zehnder, M. Düggelin, D. Mathys, R. Guggenheim, J. Vac. Sci. Technol. A 19 (2001)

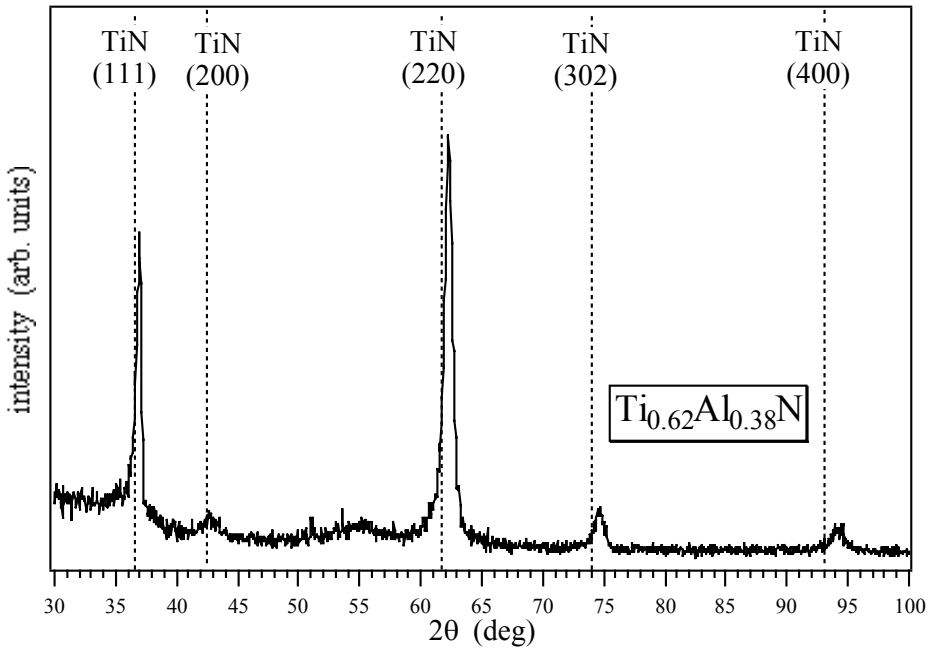

Fig. 8.2: X - ray diffraction pattern of the $Ti_{0.62}Al_{0.38}N$ film (from [SCH01a]). The sample consists exclusively of one single phase, the cubic substitutional solution (Ti,Al)N. The vertical lines indicate the peak positions for TiN. For the $Ti_{0.62}Al_{0.38}N$ sample the peaks are shifted to the large angle side, due to the shrinkage of the lattice constant by the substitution of the Ti atoms by the smaller Al atoms. The nearly complete missing of the intense (200) peak indicates a preferential orientation of the crystallites.

9 X-ray Photoelectron Spectroscopy (XPS)

Photoelectron spectroscopy is a powerful surface-sensitive technique yielding manifold information on thin film properties such as chemical composition, nature of chemical bonding and electronic valence band structure. For a comprehensive general introduction to the method see e.g. ref. [HUF96]. In a ultra-high vacuum (UHV) electron spectrometer, the sample is excited by X-rays or ultraviolet radiation, inducing the photoemission of electrons originating from the atomic layers next to the surface. An electron energy analyzer, in most cases of hemispherical geometry, allows to acquire energy spectra of the emitted photoelectrons.
Due to the larger mean electron escape depth [SEA79], X-ray electron spectroscopy (XPS) is the preferable method for the investigation *ex-situ* samples (samples being previously exposed to ambient air). Hereby the influences of surface-adsorbed molecules are thus minimized. By X-ray photoelectron spectroscopy performed at the University of Basel, the electronic core lines associated to the chemical elements can be measured from samples deposited by the sol-gel process at LESO. After subtraction of a background signal due to inelastic electron scattering in the sample [SHI72], the determination of the peak areas allows to obtain the chemical composition of the sample, either by comparison to reference samples, or by taking into account photoexcitation cross sections given in the literature [SCO76]. Examples for photoelectron spectroscopic studies on thin films (titanium containing amorphous hydrogenated carbon and titanium aluminum nitride) are described in refs. [SCH99], [SCH01b]. In order to avoid charging effects on highly insulating samples, appropriate film thickness in the order of 10 nm to 40 nm have to be used.

In preliminary experiments it could be shown that it is possible to produce sol-gel thin film samples at LESO and to measure them at the University of Basel (group Prof. Oelhafen), without breaking or contaminating them excessively during the transport (electron spectrometer: Leybold EA 10/100 MCD). A simple but effective packaging method has been devised, where the sample is hold by the edges inside an elastic tube. The sample surface remains thus untouched (important for the surface sensitive measurement technique), and additionally the fragile silicon substrate is shock-protected.

REFERENCES

[HUF96] S. Hüfner, *Photoelectron Spectroscopy: Principles and Applications*, 2nd Ed., Springer, New York (1996)

[SHI72] D. A. Shirley, Phys. Rev. B 5, 4709 (1972)

[SCO76] J. H. Scofield, J. Electron. Spectrosc. Relat. Phenom. 8, 129 (1976)

[SEA79] M.P. Seah, W.A. Dench, Surf. Interface Anal. 1, 2 (1979)

[SCH99] A. Schüler, R. Gampp, P. Oelhafen, Phys. Rev. B 60, 16164 (1999)

[SCH01b] A. Schüler, P. Oelhafen, G. Francz, T. Zehnder, M. Düggelin, D. Mathys, R. Guggenheim, Phys. Rev. B 63, 115413/1-8 (2001)

10 Summary

For the purpose of architectural integration of thermal solar collectors, special colored coatings on the collector glazing shall be developed. While aiming at a reflection in a certain variety of possible color shades, the solar transmission should be kept as high as possible. The development of a sol-gel dip-coating process for the production of suitable multilayered thin film interference stacks is supported by various measurement techniques, such as spectrophotometry, measurements of total power throughput by means of a solar simulator, spectroscopic ellipsometry, scanning electron microscopy (SEM), X-ray diffraction (XRD) and X-ray photoelectron spectroscopy (XPS).

One of the most important techniques is **spectrophotometry**, serving to characterize quantitatively the achieved colors, the color saturation and the brightness in terms of visible reflectance. These **colorimetric investigations** will allow to measure the angular dependence of the colors, and especially to test the color stability in accelerated aging tests in order to prove the durablity of the developed coatings.
From diffuse and total transmittance and reflectance spectra, as measured by means of an integrating sphere, the amount of light scattered due to defects, impurities and roughness can be determined, as well as the fraction of (unwanted) light absorption within the coating. Based on spectra of the specular transmittance and reflectance for various angles, the **optical constants n and k**, as well as the **film thickness d** can be found for individual films, which is essential for a controlled deposition of multilayers. Thin film materials will have to be tailored to match the requirements on the optical properties, and the relation of film thickness and withdrawal speed has to be characterized for each precursor solution. An even more precise tool to determine the optical material properties n and k and the film thickness d is provided by **spectroscopic ellipsometry**, This technique yields highly accurate data on the ellipsometric angles ψ and Δ, which needs to be exploited in a complex data analysis to infer the desired information.

The energy-efficiency of the colored reflection can be expressed by the ratio of the visible reflectance and the loss in solar transmission due to the collector glazing (*100% - T_{sol}*). The solar transmission of the coated glasses will be directly measured by a **solar simulator** in combination with a thermopile detector having a constant spectral sensitivity.

The coatings to be developed will have to meet high durability requirements. **Scanning electron microscopy (SEM)** will allow to obtain information on the film morphology, which is highly relevant for the optimization of the coating durability: While the production of porous films favors a low index of refraction and thus a high solar transmission, the production of dense films enhances the coating durability. Scanning electron microscopy will give insight into the nature of the coating defects (due to e.g. dust particles from air or crystallites from solution), and will thus help to achieve the goal of high quality coatings exhibiting only few defects. Detecting surface and interface roughness and in some cases also pores and voids, scanning electron microscopy will also be very helpful for the interpretation of the optical measurements. Additionally, for the controlled deposition of multilayers it will be very useful to check whether film morphology changes while adding layers, and to check layer thicknesses by cross sectional micrographs.

Another method related to durability optimization is **X-ray diffraction (XRD)**, yielding structural information such as crystalline phase identification, crystallite sizes and texture. These parameters might play an essential role for the aging performance of such coatings. The structural information will also be helpful to understand the optical material properties in terms of effective medium theories.

X-ray photoelectron spectroscopy (XPS) allows to determine the chemical composition of the deposited thin films, which can be compared to the chemical composition of the precursor solution. The correlation between the two is essential for the control of the film composition in order to establish the desired optical properties of the thin films.

An overview of the measurement techniques, the measured film properties, and the purpose of the measurements is given in Table 10.1. References to the corresponding chapters of this protocol are included.

TABLE 10.1

measurement technique	measured film property	purpose of measurement
spectrophotometry [Chapter 2] EPFL-LESO	specular reflectance and transmittance under various angles of incidence total hemispherical reflectance and transmittance diffuse hemispherical reflectance and transmittance	determination of refractive index n, extinction coefficient k and film thickness d, for controlled deposition of multilayers [Chapter 3]: control of n according to multilayer design, control of relation film thickness vs. withdrawal speed colorimetry [Chapter 4]: quantification of achieved colors, color saturation, visible reflectance (brightness of colored reflection), angle-dependence of colors, color stability in aging test measurement of light scattering
solar simulator and thermopile detector [Chapter 5] EPFL-LESO	solar transmission	direct evaluation of the transmitted energy, assessment of the energy efficiency of the colored reflection
spectroscopic ellipsometry [Chapter 6] Uni Basel, evtl. EPFL-LPCM	ellipsometric angles ψ and Δ, precise determination of refractive index n, extinction coefficient k and film thickness d	precise knowledge about optical constants n and k, dispersion relation for index of refraction, precise thickness measurement
scanning electron microscopy (SEM) [Chapter 7] EPFL-CIME	film morphology from top view and cross sectional micrographs	optimization of coating durability: production of dense films favours durability, production of porous films favors low index of refraction and thus a high solar transmission understanding of aging mechanisms by investigation of aged samples improving coating appearance: understanding nature of defects interpretation of optical measurements: surface and interface roughness, presence of pores/voids studies of multilayer formation: evolution of film morphology with increasing number of layers, check of layer thicknesses
X-ray diffraction (XRD) [Chapter 8] EPFL-LPCM	identification of crystalline phases, measurement of crystallite sizes, preferential orientation of crystallites (texture)	understanding of film structure for optimization of coating durability
X-ray photoelectron spectroscopy (XPS) [Chapter 9] Uni Basel	chemical composition	comparison of the chemical composition of the thin films with the chemical composition of the precursor solution

Table 10.1: Overview of measurement techniques, measured film properties and purpose of the measurements. References to the various chapters of this protocol are made in brackets [ ] .

Collaborations

A collaboration has been established with the research group of Prof. P. Oelhafen, Physics Department, Condensed Matter, University of Basel

Scanning investigations are foreseen in collaboration with the Prof. P. Buffat at the Interdepartemental Center of Electron Microscopy, EPFL-CIME.

Experiments of X-rays diffraction and eventually of spectroscopic ellipsometry are envisaged in collaboration with the Thin Film Physics Laboratory of Prof. F Lévy, EPFL-LPCM.

Acknowledgements

We would like to thank Prof. Peter Oelhafen and his team for the possibility of a scientific collaboration with the University of Basel, and especially Jamila Boudaden for the preparation of magnetron-sputtered thin film samples and ellipsometric measurements.

Thanks also to Pierre Loesch (EPFL-LESO) and Roland Steiner (University of Basel) for their precious technical support.

We are especially grateful to Joel Chaney (University of Nottingham, GB) and Deepanshu Dutta (University of Delhi, India) for the brilliant work they achieved during their training period at LESO (EPFL).